iScience

CellPress
OPEN ACCESS

Review

# Salt-assisted chemical vapor deposition of two-dimensional transition metal dichalcogenides

Shisheng Li[1,*]

## SUMMARY

**Salt-assisted chemical vapor deposition (SA-CVD), which uses halide salts (e.g., NaCl, KBr, etc.) and molten salts (e.g., $Na_2MoO_4$, $Na_2WO_4$, etc.) as precursors, is one of the most popular methods favored for the fabrication of two-dimensional (2D) materials such as atomically thin metal chalcogenides, graphene, and h-BN. In this review, the distinct functions of halogens (F, Cl, Br, I) and alkali metals (Li, Na, K) in SA-CVD are first clarified. Based on the current development in SA-CVD growth and its related reaction modes, the existing methods are categorized into the Salt 1.0 (halide salts-based) and Salt 2.0 (molten salts-based) techniques. The achievements, advantages, and limitations of each technique are discussed in detail. Finally, new perspectives are proposed for the application of SA-CVD in the synthesis of 2D transition metal dichalcogenides for advanced electronics.**

## INTRODUCTION

The rapid growth of technology in recent years, coupled with the emergence of artificial intelligence, the Internet of Things, and big data analytics, has led to an extremely high demand for processors with high calculation capability and speed. The traditional three-dimensional (3D) silicon semiconductor manufacturing technique is fast approaching the physical and process limits at a technology node of 2 nm. This will hinder the further development of current silicon semiconductor manufacturing techniques and prevent further scaling down. Therefore, new materials with a characteristic size of nanometer or sub-nanometer levels must be explored for application in future electronics. Atomically thin two-dimensional (2D) layered materials that demonstrate superior electrical properties could supplement 3D silicon semiconductor techniques and extend Moore's law to an ultimate technology node limit of 1 nm (Liu et al., 2021; Su et al. 2021).

The mechanical exfoliation of bulk graphite to form atomically thin graphene using scotch tape unlocked the potentials of 2D materials (Novoselov et al., 2004). New physics and applications have been developed, and even 2D transition metal dichalcogenides (TMDCs), a large family of layered compounds beyond graphene, have also been prepared using the same method (Novoselov et al., 2005). Among these exfoliated 2D TMDCs, monolayer $MoS_2$-based field effect transistors (FETs), with a record high electron mobility of ~200 $cm^2$/Vs and a high current on/off ratio of $10^8$ at room temperature, have stimulated significant research interest to study many other 2D TMDCs (Radisavljevic et al., 2011).

Although mechanical exfoliation can be used to prepare high-quality 2D materials, it cannot be used to fabricate large-area 2D materials with high yield and reproducibility. Therefore, an alternative fabrication method must be developed to synthesize 2D materials for practical applications in future electronics and optoelectronics. Chemical vapor deposition (CVD) has been widely used to fabricate one-dimensional (1D) nanowires and nanotubes since the 1990s, as it offers good controllability, high yield at low cost. Therefore, it could provide a practical solution to fabricate large-area, uniform, and high-quality 2D materials for future applications.

Salt-assisted (SA)-CVD growth of 2D materials using halide salts and molten salts has been intensively studied in recent years. In this review, the pioneering studies on the SA-CVD growth of 2D TMDCs will first be introduced, followed by clarifying the unique roles of halogens and alkali metals played in the reaction. Based on the growth mechanisms, current SA-CVD growth is categorized into two major techniques—the Salt 1.0 (halide salts-based) and Salt 2.0 (molten salts-based). Next, the applications, advantages

[1]International Center for Young Scientists (ICYS), National Institute for Materials Science (NIMS), Tsukuba 305-0044, Japan

*Correspondence: li.shisheng@nims.go.jp

https://doi.org/10.1016/j.isci.2021.103229

and limitations of each technique are reviewed systematically. Finally, the potential and challenges of using SA-CVD to fabricate 2D TMDCs for future electronics are discussed.

## Growth mechanism of halide salt-assisted CVD (HSA-CVD) of 2D TMDCs

### *Conventional CVD*

The conventional CVD setup used to grow 2D TMDCs (e.g., $MoS_2$) is illustrated in Figure 1A. In a CVD process, a crucible containing a transition metal oxide (TMO) powder and growth substrates are loaded in the high-temperature center, and chalcogen powder is loaded upstream in the low-temperature region. CVD-grown $MoS_2$ was first demonstrated in 2012 by the decomposition of $(NH_4)_2MoS_4$, and the sulfurization of a Mo film and $MoO_3$, respectively (Lee et al., 2012; Liu et al., 2012; Zhan et al., 2012). Compared to the decomposition of $(NH_4)_2MoS_4$ (which releases $H_2S$ when preparing an aqueous solution) and the deposited Mo film, stable $MoO_3$ powder offers significant feasibility for growing large $MoS_2$ monolayers with good optical and electrical qualities (Figure 1B). The growth of $MoS_2$ monolayers follows the typical vapor–solid–solid (VSS) mode. First, sulfur and $MoO_3$ powders are vaporized at sufficiently high temperatures. Second, inert carrier gas is used to transport the sulfur and $MoO_3$ vapors onto the solid growth substrates to initiate the chemical reaction (Table 1a), which leads to the nucleation and growth of solid $MoS_2$ monolayers. Later, this simple CVD growth technique using TMOs has become the dominant method not only for fabricating $MoS_2$ (Ji et al., 2013; Najmaei et al., 2013), but also for growing large variety of 2D TMDC monolayers. However, CVD presents several challenges when growing some 2D materials. For example, more critical growth conditions are required to grow $WSe_2$ monolayers (Figures 1C and 1D) (Huang et al., 2014). To generate a sufficiently large volume of $WO_3$ vapor and initiate the chemical reaction shown in Table 1b, a high temperature of >925°C and a low pressure of ~1 Torr are required to vaporize the high-melting-point $WO_3$ ($T_m$ = 1473°C), which is significantly higher than that of $MoO_3$ ($T_m$ = 795°C).

### *Role of halogens in HSA-CVD*

To enable the CVD growth of 2D TMDCs in mild conditions, the growth of large $WSe_2$ and $WS_2$ monolayers was first demonstrated via the use of alkali metal halides as growth promoters in 2015 (Figures 1E–1G) (Li et al., 2015b). By mixing tungsten oxides ($WO_{2.9}$, 1473°C) with halide salts (*AX*, *A* = Na, K; *X* = Cl, Br, I), $WSe_2$ and $WS_2$ monolayers can be grown at atmospheric pressure and significantly lower temperature of 700°C, which is more than 100°C lower than the same process using only tungsten oxide. The as-grown $WSe_2$ and $WS_2$ monolayers are free of Na contamination after rinsing in IPA/$H_2O$ solution, and show high carrier mobilities and high current on/off ratios when used as channel materials in field-effect transistors (FETs). The enhanced CVD growth of tungsten-based 2D TMDCs can be attributed to the formation of tungsten oxyhalides through reactions between tungsten oxide and halide salts at temperatures above 600°C (Table 1c). The in-situ generated tungsten oxyhalides have melting points of less than 300°C and their high vapor pressure makes them good precursors for growing high-quality $WSe_2$ and $WS_2$ monolayers in mild conditions. This mechanism is the same as the $Br_2$ and $I_2$ used in the chemical vapor transport (CVT) growth of bulk crystals, wherein the halogens facilitate the vaporization and transportation of metal precursors from the hot end to the cool end of a sealed quartz tube via the formation of volatile intermediates (Schmidt et al., 2013).

Ahead of this study, Kang et al. also reported the 4-inch wafer-scale growth of monolayer $MoS_2$ and $WS_2$ films using a metal organic (MO)-CVD system (Kang et al., 2015). They attributed the enhanced growth to the use of NaCl, KCl, and NaBr as desiccants. However, Kim et al. failed to observe enhanced growth of $MoS_2$ monolayers when more effective desiccants such as $CaCl_2$ and CaO are employed (Kim et al., 2017). Instead, they achieved the 4-inch wafer-scale growth of uniform $MoS_2$ and $WS_2$ monolayers with a large grain size of up to several tens to hundreds of micrometers through the direct spin-coating of NaCl and KI aqueous solutions onto growth substrates (sapphire). In general, the grain size of as-grown $MoS_2$ and $WS_2$ films is about 1–2 orders of magnitude larger when halide salts are employed.

### *Role of alkali metals in HSA-CVD*

Alkali metals (Li, Na, K) are important components of alkali metal halide salts which behave completely different from the halogens in the SA-CVD growth of 2D TMDCs. Their role of liquefying/stabilizing TMOs was first depicted in the vapor–liquid–solid (VLS) growth of 1D monolayer $MoS_2$ nanoribbons in 2018 (Li et al., 2018). This process is illustrated in detail in Figure 1H. First, NaCl reacts with $MoO_3$ to form a molten salt—$Na_2Mo_2O_7$ ($T_m$ = 605°C). As its melting point is below the growth temperature of 700°C and it has poor wettability on the surfaces of NaCl and $MoS_2$, the molten $Na_2Mo_2O_7$ tends to

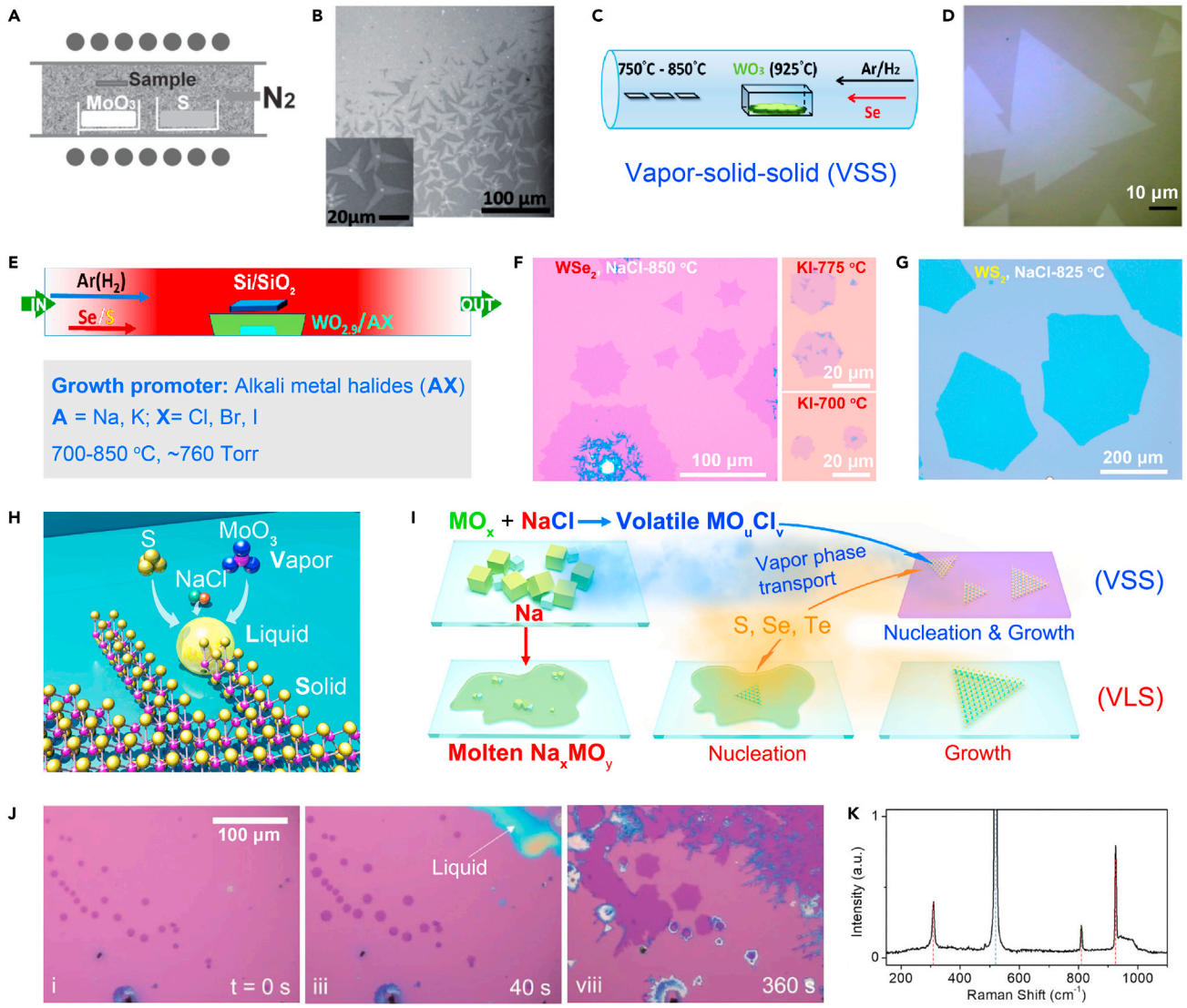


**Figure 1. Mechanism of HSA-CVD growth of 2D TMDCs**

(A and B) (A) Schematic illustration and (B) optical images of CVD-grown $MoS_2$ monolayers through sulfurization of $MoO_3$ powder. Reprinted with permission from Lee et al. (2012). Copyright 2012, John Wiley & Sons, Inc.

(C and D) (C) Schematic illustration and (D) optical image of CVD-grown $WSe_2$ monolayers through selenization of $WO_3$ powder. Reprinted with permission from Huang et al. (2014). Copyright 2014, American Chemical Society.

(E) Schematic illustration and conditions for SA-CVD growth of 2D $WSe_2$ and $WS_2$ monolayers.

(F and G) Optical images of (F) $WSe_2$ and (G) $WS_2$ monolayers fabricated through SA-CVD. Reprinted with permission from Li et al. (2015b). Copyright 2015, Elsevier.

(H) Schematic illustration of SA-CVD growth of 1D $MoS_2$ nanoribbons. Reprinted with permission from Li et al. (2018). Copyright 2018, Nature Publishing Group.

(I) Schematic illustration of the roles of the halogen and alkali metal in SA-CVD growth of 2D TMDCs. Halogens react with metal oxides to form metal oxyhalides, which facilitate the growth of 2D materials through vapor–solid–solid (VSS) mode. Alkali metals liquefy and stabilize metal oxides to form molten salts, escalating growth via vapor–liquid–solid (VLS) mode.

(J) Real time observation of the SA-CVD growth of $WSe_2$.

(K) Raman spectrum of the solidified intermediate compound, wherein the peaks marked with dashed red lines correspond to the Raman modes of $Na_2WO_4$. Reprinted with permission from Rasouli et al. (2019). Copyright 2019, Royal Society of Chemistry.

form hemispherical droplets on the surfaces. After saturation with sulfur vapor, solid $MoS_2$ monolayers are precipitated from the Na-Mo-O-S droplets (Table 1d). Besides the dominant 1D VLS growth, VSS growth also occurs owing to the presence of volatile molybdenum oxychlorides ($MoO_uCl_v$), which widens the

**Table 1. Possible reactions in CVD growth of 2D TMDCs**

| | Reactions | References |
|---|---|---|
| a. $MoS_2$ | $MoO_{3(g)} + S_{(g)} \rightarrow MoS_{2(s)} + SO_{2(g)}$ | Lee et al. (2012) |
| b. $WSe_2$ | $WO_{3(g)} + Se_{(g)} + H_{2(g)} \rightarrow WSe_{2(s)} + SeO_{2(g)} + H_2O_{(g)}$ | Huang et al. (2014) |
| c. $WSe_2$, $WS_2$ | $WO_{2.9(s)} + NaCl_{(s)} \rightarrow NaWO_{3(s)} + WOCl_{4(g)} + WO_2Cl_{2(g)} + WO_{2(s)} + W_{(s)}$<br>$WOCl_{4(g)} + WO_2Cl_{2(g)} + Se_{(g)} + H_{2(g)} \rightarrow WSe_{2(s)} + HCl_{(g)} + H_2O_{(g)}$ | Li et al. (2015b) |
| d. $MoS_2$ | $3MoO_{3(s)} + 2NaCl_{(s)} \rightarrow Na_2Mo_2O_{7(l)} + MoO_2Cl_{2(g)}$<br>$Na_2Mo_2O_{7(l)} + 7S_{(g)} \rightarrow 2MoS_{2(s)} + Na_2SO_{3(s)} + 2SO_{2(g)}$ | Li et al. (2018) |
| e. $WSe_2$ | $2WO_{3(s)} + 2NaCl_{(s)} \rightarrow WO_2Cl_{2(g)} + Na_2WO_{4(l)}$<br>$Na_2WO_{4(l)} + 2H_2Se_{(g)} + H_{2(g)} \rightarrow WSe_{2(s)} + 3H_2O_{(g)} + Na_2O_{(s)}$<br>$WO_2Cl_{2(ads)} + 2H_2Se_{(ads)} + H_{2(g)} \rightarrow WSe_{2(s)} + 2H_2O_{(g)} + 2HCl_{(g)}$ | Rasouli et al. (2019) |
| f. $TiS_2$ | $NH_4Cl_{(s)} \rightarrow NH_{3(g)} + HCl_{(g)}$<br>$2Ti_{(s)} + 2xHCl_{(g)} \rightarrow 2TiCl_{x(g)} + xH_{2(g)}$<br>$2TiCl_{x(g)} + xH_{2(g)} + 4S_{(g)} \rightarrow 2TiS_{2(s)} + 2xHCl_{(g)}$ | Gao et al. (2018) |
| g. $Nb_xW_{1-x}S_2$ | $NaCl_{(s)} + NbCl_{5(s)} \rightarrow NaNbCl_{6(s)}$<br>$WO_{3(s)} + NaCl_{(s)} \rightarrow NaWO_{3(s)} + WOCl_{4(g)} + WO_2Cl_{2(g)}$<br>$NaNbCl_{6(s)} + S_{(g)} + WOCl_{4(g)} + WO_2Cl_{2(g)} + H_{2(g)} \rightarrow$<br>$Nb_xW_{1-x}S_{2(s)} + HCl_{(g)} + H_2O_{(g)} + H_2S_{(g)}$ | Jin et al. (2019) |
| h. $Sn_xMo_{1-x}S_2$ | $SnO_{2(s)} + NaCl_{(s)} \rightarrow SnO_yCl_{z(g)} + \ldots$<br>$SnO_yCl_{z(g)} + MoO_{3(g)} + S_{(g)} \rightarrow Mo_{1-x}Sn_xS_{2(s)} \ldots$ | Mo et al. (2019) |
| i. $MoSe_2$ | $2(NH_4)_2MoO_{4(s)} \rightarrow 2MoO_{3(s)} + 4NH_{3(g)} + 2H_2O_{(g)}$<br>$2MoO_{3(s)} + 2KI_{(s)} \rightarrow MoO_2I_{2(g)} + K_2MoO_{4(l)}$<br>$MoO_2I_{2(g)} + 4H_{2(g)} + 3Se_{(g)} \rightarrow MoSe_{2(s)} + 2HI_{(g)} + 2H_2O_{(g)} + H_2Se_{(g)}$ | Kim et al. (2021) |
| j. $MoS_2$ | $Mo_{(s)} + NaCl_{(s)} + O_{2(g)} \rightarrow Na_2MoO_{4(s)} + MoOCl_{4(g)}$ | Yang et al. (2019b) |

$MoS_2$ nanoribbons (lateral growth). Consequently, contrasts of the inner and outer regions of the wide $MoS_2$ nanoribbons can be observed in the scanning electron microscope (SEM) and transmission electron microscope (TEM) images. To rule out the effects of chalcogens, the VLS growth of Mo- and W-based 2D TMDCs was confirmed through the simple sulfurization, selenization, and tellurization of molten salts—$Na_2MoO_4$ and $Na_2WO_4$, respectively (Li et al., 2018).

### *Definition of Salt 1.0 and Salt 2.0 growth techniques*

Based on the research on the HSA-CVD growth of 2D TMDCs, including the VSS growth of 2D $WSe_2$ and $WS_2$ monolayers and the VLS growth of 1D $MoS_2$ nanoribbons, the roles of halogens and alkali metals can be generalized as shown in Figure 1I. Considering NaCl—this is also applicable to other alkali metal halide salts—the halogen, Cl reacts with TMOs to form highly volatile metal oxychlorides ($MO_uCl_v$) with low-melting points (<300°C). The vapors of these metal oxychlorides can travel long distances to the growth substrates and initiate the VSS growth of 2D TMDCs. In contrast, Na reacts with TMOs to form non-volatile molten salts ($Na_xMO_y$) with high melting points (>600°C) directly on the growth substrates without vapor phase transportation. After reaction with chalcogen vapor, solid 2D TMDCs are grown from the liquid melts in the VLS mode. The coexistence of the VSS and VLS modes because of the in-situ generated $WO_2Cl_2$ and $Na_2WO_4$ was also verified through the real-time optical observation of the NaCl-assisted CVD growth of $WSe_2$ (Figures 1J and 1K, Table 1e) (Rasouli et al., 2019). Despite the coexistence of volatile metal oxyhalides and molten salts in the HSA-CVD growth of 2D TMDCs, the former plays the dominant role as effective precursors in most studies. Consequently, it is improper to refer to halide salts as molten salts, as this may lead to a misunderstanding regarding the growth mechanism.

Based on the above-mentioned growth mechanism and development of SA-CVD, it can be categorized into two growth techniques. The Salt 1.0 technique uses halide salts (*AX*, *X* = F, Cl, Br, I) as growth promoters/precursors and consists of a dominant VSS mode and an indispensable VLS mode when *A* represents alkali metals. The Salt 2.0 technique uses molten salts (e.g., $Na_2MoO_4$, $Na_2WO_4$, etc.) as growth precursors and only involves a VLS mode.

It is worth mentioning that the complex growth mechanism including the thermodynamics and kinetic processes in SA-CVD growth of 2D TMDCs must be studied further. Especially, how halogens and alkali metals

involved in the nucleation and growth of 2D TMDCs are still elusive. Although the exact chemical reactions are difficult to describe, the possible reactions proposed in related literature can be used to better understand the growth mechanism of SA-CVD (Table 1).

## Applications of HSA-CVD (Salt 1.0 technique)

Compared to the conventional CVD using TMO powders only, HSA-CVD has impressive potential for growing 2D materials under mild conditions, with better controllability, improved yield, and reproducibility. In this section, the main achievements of HSA-CVD will be discussed in the following aspects: (1) versatility; (2) doping; (3) phase; and (4) heterostructure.

### *Versatility in growing 2D materials*

The most impressive achievement of HSA-CVD is that it can be utilized to grow 47 different types of 2D materials including 32 binary metal chalcogenides (Figure 2A), $MX_2$ and MX (M = Mo, W, Re, Ti, Zr, Hf, V, Nb, Ta, Pt, Pd, Fe; X = S, Se, Te), 13 ternary and quaternary alloys, and 2 heterojunctions (Zhou et al., 2018). Pure metals, such as Ta and Re, have also been directly mixed with NaCl or KI to grow Ta- and Re-based 2D TMDCs. The use of mixed metal–halide salt precursors provides a more reliable strategy instead of using their non-stable, highly volatile, toxic halides. For instance, Gao et al. grew semi-metallic $TiS_2$ using mixed Ti–$NH_4Cl$ instead of titanium chlorides (Table 1f) (Gao et al., 2018).

Owing to its versatility, feasibility, and reproducibility, the HSA-CVD method (Salt 1.0 technique) has even been used to grow sensitive 2D TMDCs without using molecular beam epitaxy under vacuum conditions. Wang et al. reported on the simple CVD growth of high-quality 2D superconducting $NbSe_2$ monolayers using $NbO_x$-NaCl and charge density wave conductor–$TiSe_2$ using $TiO_x$-LiCl, respectively (Wang et al., 2017a, 2018). The advantage of using partially oxidized metal powders (e.g., $NbO_x$, $TiO_x$) is that the release rate and amount of in-situ generated metal oxychlorides can be controlled effectively. Besides 2D layered crystals, Hu et al. reported on the halide salt-induced self-limited growth of ultrathin Ge flakes using a GeS-KCl mixture (Hu et al., 2018). As shown in Figure 2B, the successful growth of non-layered Ge flakes can be primarily attributed to preferential growth of the lowest formation energy (111) plane and the giant interface distortion caused by the Cl-Ge motif.

Beside the widely used metal chlorides, bromides and iodides, metal fluorides were also employed for enhanced CVD growth of 2D materials until very recently. In 2019, Liu et al. demonstrated fast and enhanced CVD growth of graphene on copper foils that were placed on fluoride substrates (Figure 2C) (Liu et al., 2019). This was an important addition to the research on HSA-CVD as it confirmed the inclusion of fluorides ($MF_2$, M = Mg, Ca, Ba) as effective growth promoters. Large graphene films with a lateral size of ~1 mm can be grown at a fast rate of ~200 μm/s (Figure 2D). The rapid growth can be attributed to the released $F_2$, which lowers the dissociation energy of $CH_4$ to a more active carbon species. Fluorides also promote the growth of h-BN, $WS_2$, and $MoSe_2$. Therefore, HSA-CVD is a versatile fabrication method, not only for 2D metal chalcogenides, but also for graphene and h-BN.

Later, Chang et al. deposited trilayer NaF–$SiO_2$–$MoO_3$ films on sapphire substrates to realize the fast growth of large monolayer and bilayer $MoS_2$ (1.1 mm/200 μm) in 10 min, and fabricated fully covered films on centimeter-scale substrates that had a record-high average grain size of 450 μm (Chang et al., 2020). As illustrated in Figure 2E, $MoO_3$ can diffuse through the cracks in the thin $SiO_2$ layer and initiate the reaction between NaF and $MoO_3$ to generate molten $Na_2Mo_2O_7$ and volatile $MoO_2F_2$ vapor. The molten $Na_2Mo_2O_7$ can keep diffusing on the surface of the NaF layer and grow into large droplets with a prolonged reaction time. Therefore, the growth of monolayer, bilayer, and even trilayer $MoS_2$ can be achieved by initializing the sulfurization of $Na_2Mo_2O_7$ droplets at different growth stages.

### *Doping*

Doping heteroatoms into host materials can effectively modify their crystal and electronic structures, and significantly improve their electrical, optical, magnetic, and catalytic properties. In recent years, a significant amount of research has been conducted on the CVD growth of doped 2D TMDCs. However, if the melting points and vapor pressures of the host and dopant metal precursors differ significantly, it is hard to simultaneously vaporize both metal precursors during the CVD process. While HSA-CVD plays an important role in growing doped 2D TMDCs. For instance, Nb-doped $WS_2$ monolayers were grown using a mixed $WO_3$–Nb–NaCl precursor; atomic resolution STEM revealed that the substitutional doping of

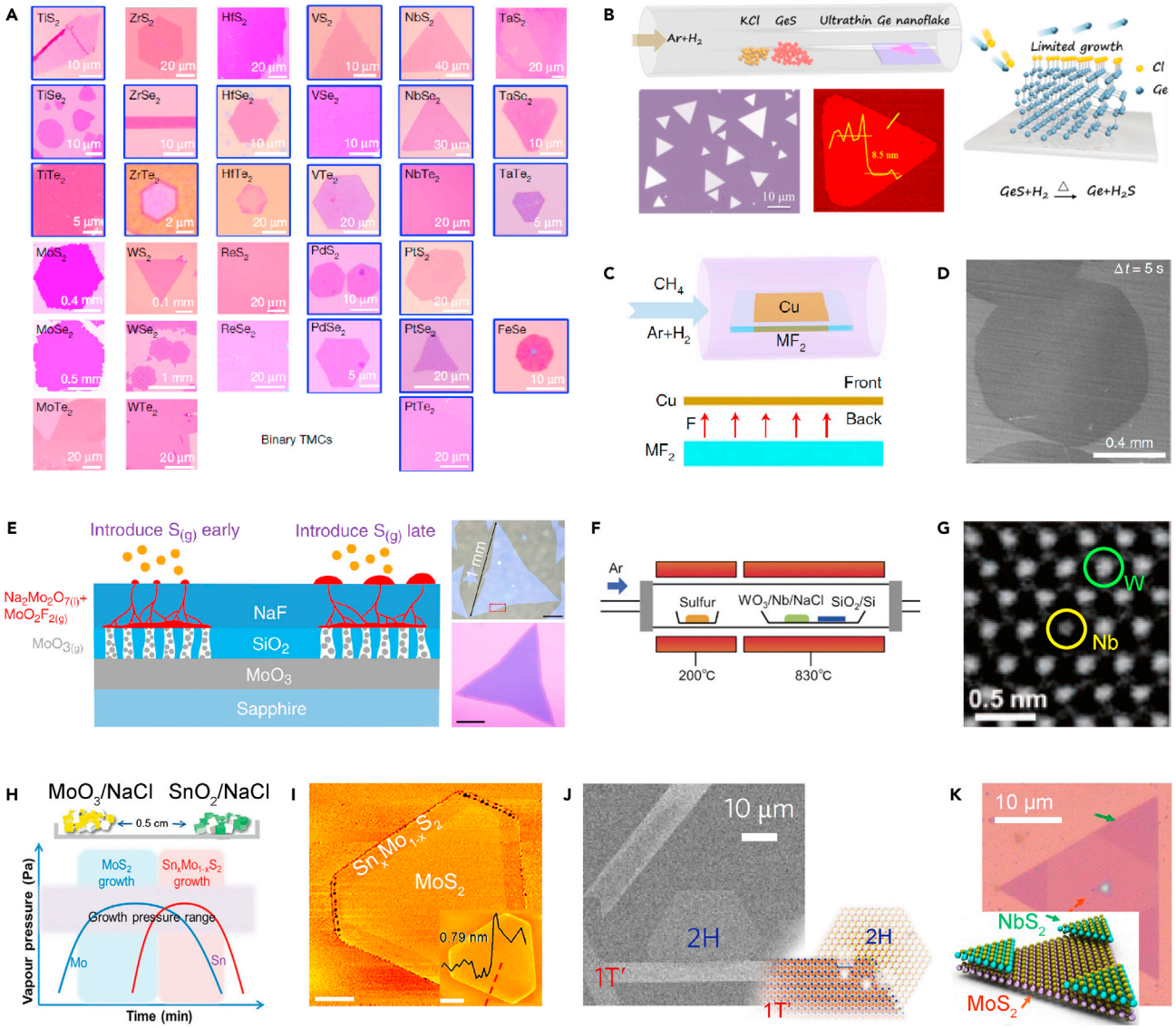


**Figure 2. Applications of HSA-CVD (Salt 1.0 technique)**

(A) Library of atomically thin metal chalcogenides grown using HSA-CVD. Reprinted with permission from Zhou et al. (2018). Copyright 2018, Nature Publishing Group.

(B) Halide-induced self-limited growth of non-layered Ge thin flakes using GeS-KCl as precursors. Reprinted with permission from Hu et al. (2018). Copyright 2018, American Chemical Society.

(C) Schematic illustration of fluoride-assisted CVD growth of graphene.

(D) SEM image of ~1 mm graphene grown on copper foil in 5 s. Reprinted with permission from Liu et al. (2019). Copyright 2019, Nature Publishing Group.

(E) Schematic illustration and optical images of the rapid CVD-grown large, layer-number tunable $MoS_2$ using a self-capping VLS method. Reprinted with permission from Chang et al. (2020). Copyright 2020, Nature Publishing Group.

(F) Schematic illustration of the growth of Nb-doped $WS_2$ monolayers using $WO_3$–Nb-NaCl as a precursor.

(G) Atomic-resolution STEM image of the substitutional doping of Nb at W site. Reprinted with permission from Sasaki et al. (2016). Copyright 2016, The Japan Society of Applied Physics.

(H) Vapor pressure evolution of TM precursors for the sequential growth of $MoS_2$ and $Sn_xMo_{1-x}S_2$ using separated $MoO_3$–NaCl and $SnO_2$–NaCl.

(I) AFM image of the as-grown $MoS_2$–$Sn_xMo_{1-x}S_2$ in-plane heterojunction. Reprinted with permission from Shao et al. (2020). Copyright 2020, The Authors.

(J) Phase controlled growth of 2H-1T′ $MoTe_2$ in-plane junctions using $MoO_3$–NaCl. Reprinted with permission from Sung et al. (2017). Copyright 2017, Nature Publishing Group.

(K) Optical image of vertical $NbS_2$–$MoS_2$ heterojunction through one-step sulfurization of the separated $MoO_3$ and $Nb_2O_5$–NaCl. Reprinted with permission from Fu et al. (2018b). Copyright 2018, American Chemical Society.

Nb occurred at the W sites in the $WS_2$ monolayers (Figures 2F and 2G) (Sasaki et al., 2016). With small Nb dopants (~0.5 atom%), new broad photoluminescence (PL) emissions occurred at 1.4–1.6 eV in addition to the PL emission of $WS_2$ monolayers at ~1.98 eV. Mixed $WO_3$–$NbCl_5$–NaCl has also been used to grow Nb-doped $WS_2$ monolayers (Table 1g) (Jin et al., 2019; Tang et al., 2021). Compared to Nb, $NbCl_5$ has a higher doping ability owing to its lower melting point and higher vapor pressure. Similarly, Eu-doped $MoS_2$ ($Eu_2O_3$–NaCl) (Xu et al., 2018), V-doped $MoS_2$ ($Mo_6V_9O_{40}$–NaCl) (Zhang et al., 2020), Fe/Co/Mn-doped $MoS_2$ ($MoO_3$ + $Fe_3O_4$/CoO/$MnO_x$–NaCl) (Cai et al., 2020; Li et al., 2020b), and Sn-doped $MoS_2$ ($MoO_3$ + $SnO_2$–NaCl) (Table 1h) (Mo et al., 2019) have also been successfully grown using NaCl as a growth promoter. In principle, the doping concentration can be tuned by varying the ratio of the metal precursors. However, in reality, it is quite challenging to simultaneously vaporize the metal precursors at a fixed rate and guarantee the uniform spatial distribution of the metal precursor vapors. Consequently, it is difficult to grow uniformly doped 2D TMDCs with the desired doping concentration and properties. Nevertheless, Shao et al. exploited the sequential vaporization of metal precursors to grow lateral $MoS_2$–$Sn_xMo_{1-x}S_2$ in-plane heterojunctions using separated $MoO_3$–NaCl and $SnO_2$–NaCl as precursors (Shao et al., 2020). As the melting point of $MoO_3$ ($T_m$ = 795°C) is much lower than that of $SnO_2$ ($T_m$ = 1630°C), the in-situ generated $MoO_uCl_v$ vapor initiated the growth of the inner $MoS_2$ layer first, and the later generated $SnO_mCl_n$ and $MoO_uCl_v$ vapors result in the growth of outer $Sn_xMo_{1-x}S_2$ layer (Figures 2H and 2I).

### *Phase*

The phase of 2D TMDCs represents their polymorphism. Based on their atomic structures, monolayer 2D TMDCs have mainly 1H, 1T, and 1T′ phases. These phases provide various electrical, optical, and catalytic properties to 2D TMDCs. For instance, semiconducting 1H-TMDCs are primarily used as channel materials in FETs or optoelectronic devices (Wang et al., 2012), whereas metallic 1T′-TMDCs can be used as high-performance contacts in TMDC-based FETs (Kappera et al., 2014) and catalytic electrodes for hydrogen evolution (Voiry et al., 2013). Consequently, phase conversion and phase-controlled synthesis of metastable 1T′-TMDCs have received significant attention in recent years (Lai et al., 2021; Liu et al., 2018; Voiry et al., 2015; Yu et al., 2018). HSA-CVD has been widely used to grow phase-controlled 2D TMDCs. For instance, 1T′-$MoTe_2$ was grown through the tellurization of $MoO_2$–KI (Zhang et al., 2017b). Coplanar semiconducting-metallic 2H-1T′ $MoTe_2$ in-plane junctions were grown using $MoO_3$–NaCl by varying the growth temperatures (Figure 2J) (Sung et al., 2017). This unique CVD-grown heterojunction was able to provide a reduced Schottky barrier and improved electrical contacts in 2H-1T′ $MoTe_2$-based FETs. Similarly, phase-selective 1H- and 1T′-$MoS_2$ and their heterojunctions have been grown by the sulfurization of $MoO_2$–KCl and the decomposition of $K_2MoS_4$, respectively (Arreola et al., 2021; Liu et al., 2018). In these studies, the strong electron doping effect of alkali metals play vital important role. Only the surface adsorbed alkali metals to some extent, the formation energy of 1T′ phase was smaller than that of 1H phase. Furthermore, Shao et al. reported that KX (X = Cl, Br, I) is preferable for growing 1T-$SnS_2$, whereas NaX is more suitable for growing 2H-$SnS_2$ (Shao et al., 2019). Therefore, the alkali metal halide salts and growth conditions (e.g., temperatures, $H_2$ concentration, etc.) must be carefully chosen and tuned to achieve phase-selective growth of 2D TMDCs.

### *Heterojunctions*

Heterostructures (in-plane and vertical) can be assembled using two or more 2D TMDCs to introduce new properties compared to individual components (Tan et al., 2021). Based on the electrical properties of 2D TMDCs—metals (M) and semiconductors (S), two main M–S and S–S heterojunctions are intensively studied. M–S junctions are primarily grown for contact engineering of 2D TMDC-based FETs (Li et al., 2020a), whereas S–S type TMDC-based PN junctions have significant potential for application in solar cells, photodetectors, and light emission devices (Furchi et al., 2014; Lee et al., 2014; Li et al., 2015a). However, it is difficult to grow high-quality TMDC-based heterojunctions with arbitrary combinations. During the sequential growth of different 2D TMDCs at high temperatures (>600°C), severe degradation is inevitable, especially for heterojunctions with different chalcogens. This is primarily because the stability of different 2D TMDCs varies (sulfides > selenides > tellurides). Nevertheless, HSA-CVD has been employed to lower the growth temperature and maintain the grown 2D TMDCs intact. As shown in Figure 2K, vertical $MoS_2$–$NbS_2$ junctions were achieved through one-step sulfurization of separated $MoO_3$ and $Nb_2O_5$–NaCl (Fu et al., 2018b). Similarly, $WS_2$–$NbS_2$ in-plane junctions were obtained through the sequential growth of $WS_2$ and $NbS_2$ using $WO_3$ and $Nb_2O_5$–NaCl (Zhang et al., 2018). $MoS_2$–$WS_2$ in-plane junctions were also grown via NaCl-assisted simultaneal sulfurization of separated $MoO_2$ and $WO_3$ powders (Wang et al., 2017b). The above-mentioned heterojunctions are still poor in controlling the geometric configuration

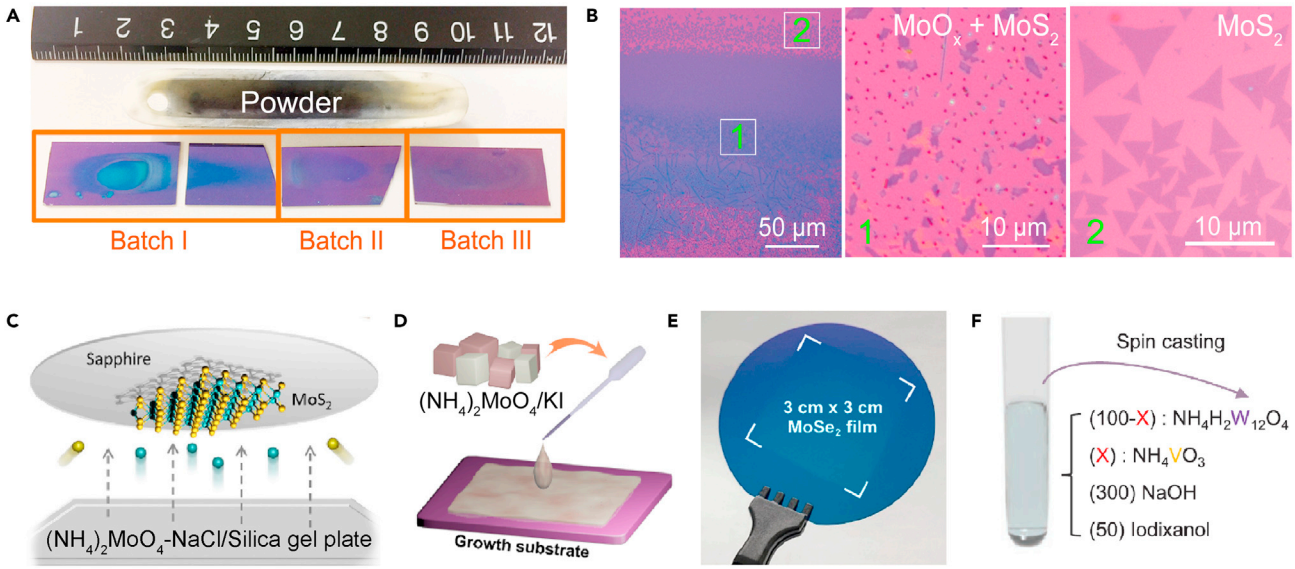


**Figure 3. Evolution of HSA-CVD**

(A) Poor batch-to-batch reproducibility in the CVD growth of $MoS_2$ through the sulfurization of $MoO_3$ powder.

(B) Optical images of as-grown $MoS_2$ on $SiO_2$/Si with inevitable byproduct contamination. Reprinted with permission from Li et al. (2019). Copyright 2019, Royal Society of Chemistry.

(C) Schematic illustration of the growth of wafer-scale $MoS_2$ using $(NH_4)_2MoO_4$–NaCl-coated silica gel plate. Reprinted with permission from Wang et al. (2020). Copyright 2020, American Chemical Society.

(D and E) (D) Schematic illustration of depositing $(NH_4)_2MoO_4$–KI liquid precursor to grow (E) a large-area monolayer $MoSe_2$ film. Reprinted with permission from Kim et al. (2021). Copyright 2021, American Chemical Society.

(F) Schematic illustration of the liquid precursor for growing monolayer V-doped $WSe_2$ flakes. Reprinted with permission from Fan et al. (2020). Copyright 2019, The Authors.

and components. To satisfy their application in electronics, more efforts should be devoted to developing low-temperature growth techniques for high-quality 2D TMDC-based heterojunctions.

## Upgrading of HSA-CVD (Salt 1.0 + technique)

Despite its numerous advantages, HSA-CVD (Salt 1.0 technique) also has multiple drawbacks. One severe issue is the excessive and non-uniform vapors of the transition metal (TM) precursors in the growth chamber, because of which the growth of 2D TMDCs strongly relies on the position of the substrates. Figure 3A shows the different deposition patterns on growth substrates in three different batches (Li et al., 2019). In addition to the desired 2D TMDC monolayers, inevitable byproducts such as TMOs and thick 2D TMDCs were also deposited on the growth substrates, severely hindering the application of CVD-grown 2D TMDCs (Figure 3B). Moreover, these byproducts can contaminate the crucibles and growth chambers, which must be cleaned or replaced frequently, thereby increasing the production cost. To overcome these detrimental effects of TMO powders, alternative soluble TM precursors in aqueous solutions can be employed to minimize their use in SA-CVD. For example, large-area monolayer and few-layer 1T′-$MoTe_2$ (~1 mm) and 1T′-$WTe_2$ (~350 μm) were grown using $(NH_4)_6Mo_7O_{24}$–KCl and $(NH_4)_{10}W_{12}O_{41}$–KCl aqueous solutions (Chen et al., 2017b). Phase-selective 2H- and 1T′-$MoTe_2$ were grown using soluble $(NH_4)_6Mo_7O_{24}$–NaCl as a precursor by modulating the growth temperature (Hoang et al., 2018). Two-inch wafer-scale pristine and Re-doped $MoS_2$ monolayers were grown using soluble $(NH_4)_2MoO_4$–NaCl as a host precursor and solid $ReCl_3$ powder as the dopant precursor (Figure 3C) (Wang et al., 2020). Dirac semi-metallic $PtTe_2$ flakes with ultrahigh conductivity were epitaxially grown on mica using soluble $PtCl_4$–NaCl (Fu et al., 2018a). Unlike the direct load of a large amount of mixed TMO-halide salt powders in crucibles, the mixed TM precursor-halide salt can be deposited more uniformly by drop-casting their aqueous solutions into crucibles or onto a silica gel plate. Therefore, these crucibles/silica gels can release TM precursors more uniformly in the typical CVD process, resulting in more uniform 2D TMDCs with high growth reproducibility. However, the crucibles/silica gels still undergo contamination, making it difficult to clean and reuse them.

Alternatively, the aqueous solutions of mixed precursors, such as $(NH_4)_2MoO_4$–KI, $(NH_4)_2WO_4$–KI, and $(NH_4)_6Mo_7O_{24}$–NaCl, were directly spin-coated on growth substrates to grow wafer-scale 2D TMDCs (Figures 3D and 3E) (Kim et al., 2021; Zhang et al., 2021a). However, these ammonia molybdates/tungstates have poor thermal stability and provide a low yield of 2D TMDCs. During the CVD process, the ammonia molybdates/tungstates first decompose to form $MoO_3$/$WO_3$ and release $NH_3$ at temperatures of above 100°C. Only when mixed with a proper amount of alkali metal halide salts, large-area continuous TMDC films can be grown successfully. Although these studies attribute this high-efficiency growth to the formation of volatile TM oxyhalides (Table 1i), the contribution of the alkali metals that can liquefy and stabilize TMOs during the HSA-CVD process should not be ignored. The importance of alkali metals is further verified by pre-deposition of sodium cholate (without halogens) on growth substrates to promote the growth of $MoS_2$, 1T′-$MoTe_2$, and 1T′-$WTe_2$ (Han et al., 2015; Naylor et al., 2016, 2017) using $(NH_4)_6Mo_7O_{24}$ and $(NH_4)_6H_2W_{12}O_{40}$ aqueous solutions, respectively. Similarly, NaOH can also be mixed with $(NH_4)_6H_2W_{12}O_{40}$ and $NH_4VO_3$/$C_4H_4NNbO_9$ in aqueous solutions to enhance the growth of V/Nb-doped $WSe_2$ (Figure 3F) (Fan et al., 2020; Vu et al., 2021; Yun et al., 2020). Therefore, alkali metals play a more significant role than halogens in stabilizing the soluble TM precursors on growth substrates and enhancing the growth of 2D TMDCs. In addition, the in-situ generated volatile TM oxyhalides have minimal impact to the growth environments due to limited loading amount of soluble TM precursors on growth substrates.

## Applications of molten salt-CVD (Salt 2.0 technique)

In contrast to the Salt 1.0 technique with its complex VSS and VLS growth modes, the Salt 2.0 technique uses molten salts to grow 2D TMDCs in the VLS mode. To guarantee the success of the Salt 2.0 technique, the molten salts must meet three main criteria (Figure 4A): (1) reasonably high melting points; (2) ability to form stable melts with a low vapor pressure at CVD growth temperatures; and (3) soluble in $H_2O$. The first two criteria ensure the VLS growth of 2D TMDCs, whereas the third criterion can ensure the deposition of molten salts through easy methods such as spin coating, drop casting, ink-jet printing, and so forth. Fortunately, a large group of molten salts with a chemical formula of $A_xMO_y$ (*A*-alkali metals; *M*-transition metals) can be used as precursors to grow 2D TMDCs. Some of these, such as $Na_2MoO_4$ and $Na_2WO_4$, have been proved to be ideal precursors, and have been widely used to grow Mo- and W-based 2D TMDCs (Cun et al., 2019; Li et al., 2018; Ma et al., 2021). Spin coating of their aqueous solutions is the most used method to deposit molten salts on growth substrates (Figure 4B). To guarantee the uniform deposition of molten salts, the surface of growth substrates must be hydrophilic. Therefore, UV-$O_3$, oxygen plasma and piranha solution can be utilized to treat the growth substrates. In addition, by varying the concentration of the molten salt solutions and the spin-coating rate, the amount of deposited molten salt can be varied. Consequently, the surface coverage, domain size, and layer numbers of the TMDC flakes/films can be engineered. Recently, 2-inch wafer-scale monolayer $MoS_2$ and $WS_2$ films were successfully grown with spin-coated $Na_2MoO_4$ and $Na_2WO_4$ aqueous solutions on sapphire and $SiO_2$/Si substrates, respectively (Figures 4C–4F) (Li et al., 2019; Liu et al., 2020). Considering the CVD growth of 2D $MoS_2$ monolayers using the Salt 2.0 technique, spin-coated $Na_2MoO_4$ particles are first melted by heating them up to the growth temperature, ~750°C, which is above its melting point. Owing to the low vapor pressure of $Na_2MoO_4$ (Kazenas et al., 2010), stable $Na_2MoO_4$ melts have good wettability on $Al_2O_3$ and $SiO_2$/Si substrates are formed (Figure 4C). After adsorbing sulfur vapor, solid $MoS_2$ monolayers are precipitated from the sulfur-saturated Na-Mo-O-S melts as illustrated in Figure 1I. Furthermore, monolayer $MoS_2$ arrays can be successfully grown using patterned $Na_2MoO_4$, which cannot be achieved with volatile $MoO_uCl_v$ and $MoO_3$ without using pre-deposited nucleation seeds.

Although the Salt 2.0 technique is well-suited to growing wafer-scale monolayer $MoS_2$ and $WS_2$ films, it is still difficult to grow large-area transition metal selenides and tellurides. Recently, a mixed transition metal salt and chalcogen salt, $Na_2MoO_4$–$Na_2SeO_3$ was developed to achieve a wafer-scale growth of monolayer $MoSe_2$ film with a grain size of 100–250 μm and unprecedented uniformity (Figure 4G) (Li et al., 2021b). The enhanced growth of $MoSe_2$ can be attributed to the direct formation of intermediate Na-Mo-O-Se melts from the mixed $Na_2MoO_4$–$Na_2SeO_3$. Compared to Na–Mo–O melts, the Na–Mo–O–Se melts are a step closer to the final $MoSe_2$ monolayers, and consequently, it kinetically favors the nucleation and growth of $MoSe_2$ monolayers. It is also applicable for the enhanced growth of 2D $ReSe_2$ and $WTe_2$ using mixed $NaReO_4$–$Na_2SeO_3$ and $Na_2WO_4$–$Na_2TeO_3$, respectively. Therefore, using mixed molten transition metal and chalcogen salts is a versatile option for growing large groups of 2D TMDCs and is an important upgrade to the Salt 2.0 technique.

Besides the growth of large-area wafer-scale binary 2D TMDCs, the Salt 2.0 technique also provides great controllability for growing doped/alloyed 2D TMDCs using mixed salt aqueous solutions instead of powdered

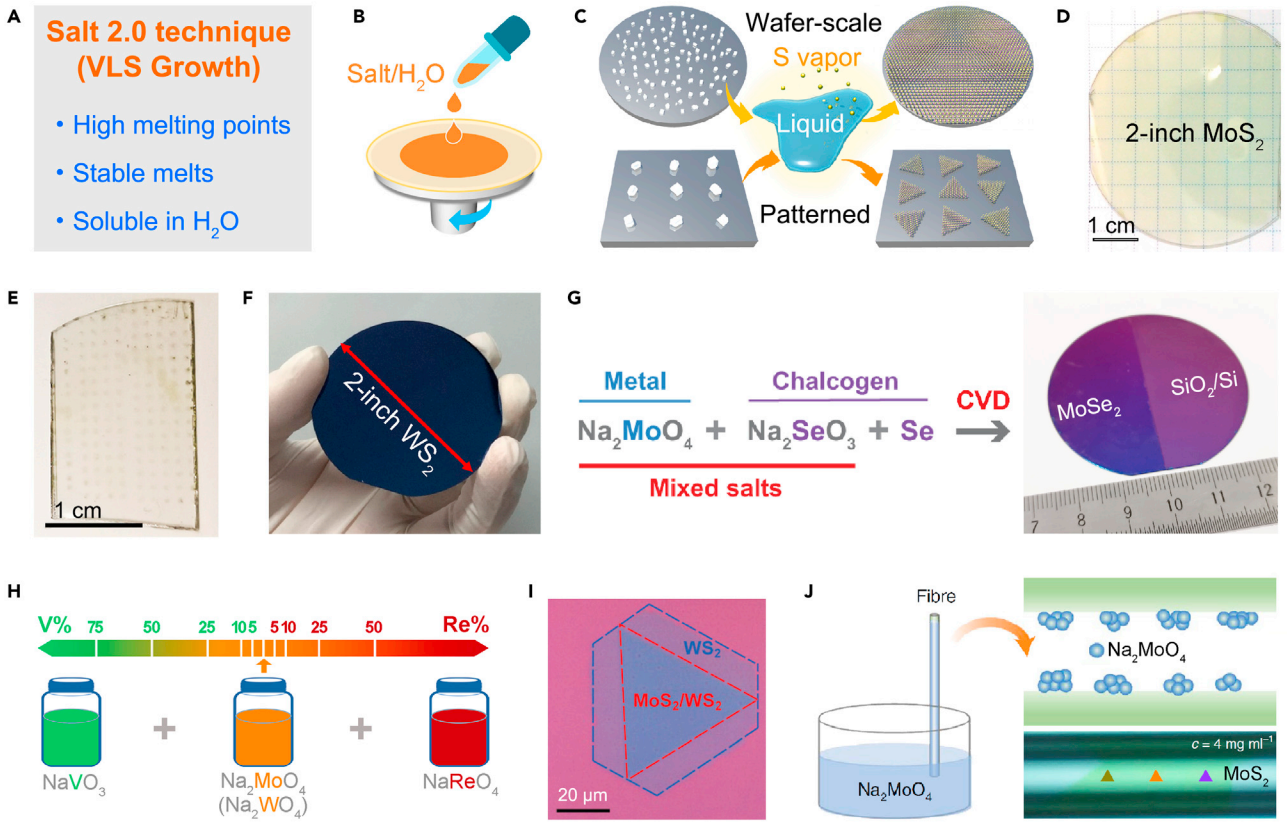


**Figure 4. Application of molten salt-CVD (Salt 2.0 technique)**

(A) Three main criteria for Salt 2.0 technique.

(B) Schematic illustration of the deposition of molten salt onto a growth substrate through spin-coating of its aqueous solution.

(C) Schematic illustration of a wafer-scale and patterned growth monolayer $MoS_2$ film using $Na_2MoO_4$ as a precursor.

(D and E) Optical images of (D) 2-inch monolayer $MoS_2$ film and (E) patterned $MoS_2$ array grown on sapphire substrates. Reprinted with permission from Li et al. (2019). Copyright 2019, Royal Society of Chemistry.

(F) 2-inch wafer-scale monolayer $WS_2$ film grown on $SiO_2$/Si substrate using $Na_2WO_4$ as a precursor. Reprinted with permission from Liu et al. (2020). Copyright 2020, American Chemical Society.

(G) Enhanced growth of 2-inch wafer-scale monolayer $MoSe_2$ film using mixed $Na_2MoO_4$–$Na_2SeO_3$ as precursor. Reprinted with permission from Li et al. (2021b).

(H) Schematic illustration of Re- and V-doped 2D TMDCs grown using mixed molten salts with tunable compositions. Reprinted with permission from Li et al. (2021a). Copyright 2021, John Wiley & Sons, Inc.

(I) An optical image of a $MoS_2$–$WS_2$ vertical heterojunction grown with separated $Na_2MoO_4$ and $Na_2WO_4$. Reprinted with permission from Bai et al. (2021). Copyright 2021, The authors.

(J) Conformal growth 2D TMDCs in optic fiber for super-high nonlinearity. Reprinted with permission from Zuo et al. (2020). Copyright 2020, Nature Publishing Group.

precursors. Recently, tunable doping of rhenium (Re) and vanadium (V) into 2D $MoS_2$, $WS_2$, and $WSe_2$ monolayers was achieved using $Na_2MoO_4$ and $Na_2WO_4$ as the host salts, and $NaReO_4$ and $NaVO_3$ as the dopant salts (Figure 4H) (Li et al., 2021a). The stable mixed molten salts provide high flexibility in tuning the doping concentration across a wide range by varying the dopant salt concentration, which is quite challenging in a typical VSS growth process. For instance, Zou et al. grew V-doped $MoS_2$ films with a wide doping concentration of 0.3–11.3 atom% (Zou et al., 2021). This was achieved only through the use of vanadium precursors with various doping abilities ($V_2O_5$ < $NH_4VO_3$ < $VCl_3$). As Re and V are neighbors of Mo and W in the periodic table, they act as electron donors and acceptors when substitutional doping at the Mo and W sites in 2D TMDCs, respectively. Therefore, Re and V doping can effectively modify the carrier types and concentrations of 2D TMDCs. The optical and electrical properties of Re- and V-doped 2D TMDCs can be precisely tuned by varying the composition of the mixed salt precursors. In particular, heavily V-doped $WS_2$ and $WSe_2$ exhibit a significant increase in electrical conductivity, up to $10^8$ times, compared to the intrinsic samples. Therefore, they are ideal

van der Waals contacts for p-type 2D TMDC-based FETs. Similarly, Qin et al. grew Nb-doped $WS_2$ monolayers using a mixed $Na_2WO_4$–$Nb(HC_2O_4)_5$ aqueous solution, and achieved a high Nb doping density of $10^{14}$ $cm^{-2}$ (Qin et al., 2019). These studies have demonstrated that the Salt 2.0 technique using mixed molten salts are not only limited to TM salts, but can also employ chalcogen salts to provide an effective method of growing large groups of doped/alloyed 2D TMDCs with multiple metal and chalcogen components in the form of $(M_uM'_vM''_w \ldots)(S_xSe_yTe_{1-x-y})_2$. Not limited to the doped/alloyed 2D TMDCs using mixed molten salts, $Na_2MoO_4$ and $Na_2WO_4$ deposited on separated substrates can even enable the single-step CVD growth of $MoS_2$–$WS_2$ vertical heterojunctions (Figure 4I) (Bai et al., 2021). This further demonstrates the applications of molten salts for diverse structures of 2D TMDCs.

One more advantage of using aqueous solution is the possible coating of molten salt on the surfaces with arbitrary shape and even the inner chamber of an object. This can further extend the growth/integration of 2D TMDCs to many other functional devices. Recently, Zuo et al. reported on the conformal growth of 2D TMDCs in the channels of optical fibers (Zuo et al., 2020). As shown in Figure 4J, a $Na_2MoO_4$ aqueous solution was first filled in the inner channels of optical fiber and dried. After sulfurization of the molten salts using low-pressure CVD, $MoS_2$ monolayers were conformally grown inside the optical fibers. The coverage of the $MoS_2$ monolayers can be easily engineered by tuning the concentration of the $Na_2MoO_4$ aqueous solution. This simple method can also be applied to grow $MoSe_2$ and $WS_2$ inside the optical fibers. With this novel integration of 2D TMDCs and optical fibers, ultrahigh non-linear optical properties that are several hundred times higher than those of TMDC monolayers on flat substates were achieved.

Overall, the Salt 2.0 technique using molten salts is still in its infancy stage. However, it has clearly demonstrated its efficacy in growing large-area wafer-scale 2D TMDC polycrystalline film, patterns, alloys, and heterojunctions. Furthermore, by using a minimal amount of molten salt, the Salt 2.0 technique can reduce the burden on the growth chambers, and significantly reduce the likelihood of contamination.

## Alkali metals—two sides of the same coin

Regardless of the technique used, alkali metals are the indispensable component that promotes lateral growth of the 2D TMDCs. Numerous alkali metal-based chemicals such as NaOH, KOH, $Na_2SO_4$, $KH_2PO_4$, $Na_2CO_3$, $KNO_3$, $CH_3COONa$, $C_6H_5O_7Na_3$, PTAS, EDTA-4Na, etc., can be employed to enhance the CVD growth of 2D TMDCs (Ling et al., 2014, 2016; Song et al., 2017; Wang et al., 2019a; Yang et al., 2019a). However, the alkali metals may on one hand contaminate the TMDCs grown, leading to inferior device performance, poor stability, and even failure of the electronic devices. Therefore, it is vital to maximize the beneficial effects of alkali metals in facilitating growth, while minimizing their negative impacts on downstream applications. To achieve this, (i) the detailed roles and chemical states of the alkali metals in the CVD process, and (ii) their distribution on the 2D TMDCs and growth substrates must be understood. With that, a comprehensive evaluation of the impacts of alkali metals on the as-grown 2D TMDCs can be performed, and an alkali metal removal strategy can be developed.

When 2D TMDCs are grown using the HSA-CVD process (Salt 1.0 technique), halide salt particles are often found at edges of the as-grown TMDCs. As shown in Figure 5A, NaBr nanoparticles accumulated at the periphery of the as-grown $MoS_2$ monolayers that were grown using $MoO_2$-NaBr. Li et al. claimed that NaBr enables the synthesis of $MoS_2$ monolayers through a surfactant-mediated growth mechanism without forming molten salts. The Na ions in NaBr chemically passivate the edges of the growing $MoS_2$ monolayers, relaxing the in-plane strain to suppress vertical growth and promote lateral growth (Li et al., 2020c). In contrast, Huang et al. attributed the rapid, high-quality, and controllable growth of $MoS_2$ monolayers to a new vapor–liquid–adatom–solid (VLAS) growth mode (Huang et al., 2020), where catalytic KCl particles synergistically capture $MoO_x$ and S vapors. Oversaturated adatoms subsequently diffuse along the edges to resume the lateral growth of the $MoS_2$ monolayers (Figure 5B).

Despite the different growth mechanisms proposed, the alkali metal ions distribute basically all over the growth substrates and even underneath the as-grown 2D TMDCs due to the strong chemical affinity with oxide substrates (Figure 5C) (Han et al., 2021; Li et al., 2020c; Zhang et al., 2018). Because of the presence of these alkali metal ions at the TMDC-substrate interface, 2D TMDCs grown using SA-CVD can be wet transferred with or without the mediation of a coated polymer (e.g., PMMA, PC, etc.) film in de-ionized (DI) $H_2O$. Compared to the use of corrosive and toxic etchants, such as HF, NaOH, and KOH, DI $H_2O$ provides a fast damage-free transfer process for SA-CVD grown 2D TMDCs (Kojima et al., 2019; Zhang et al.,

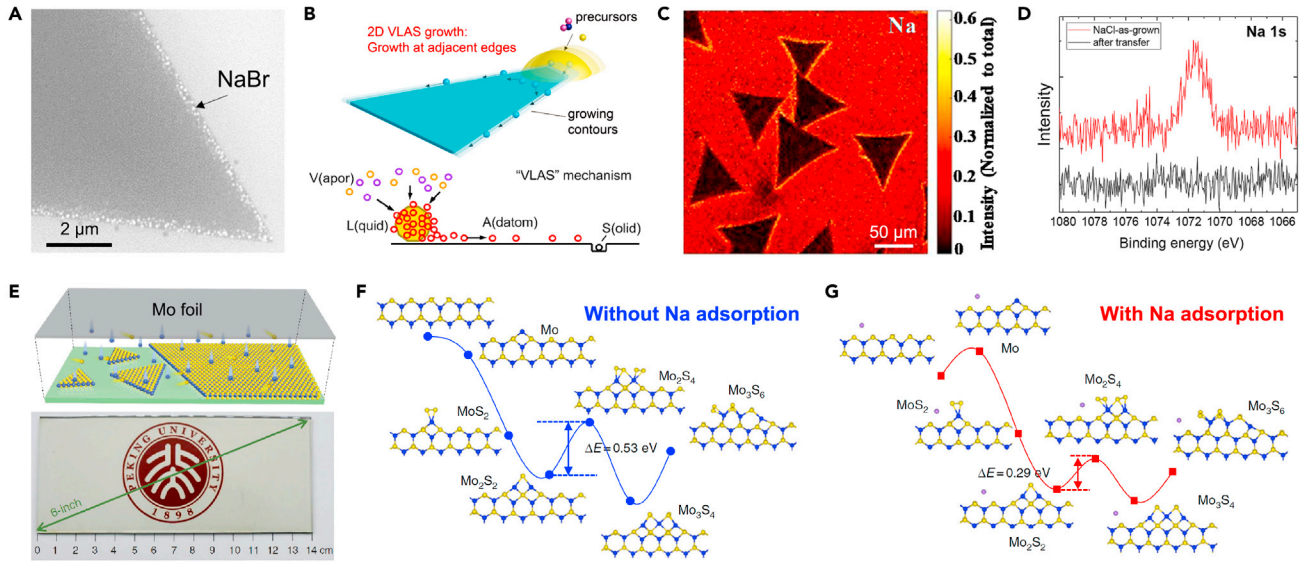


**Figure 5. Alkali metals in the CVD growth of 2D TMDCs**

(A) SEM image of NaBr nanoparticles on the edges of a $MoS_2$ monolayer. Reprinted with permission from Li et al. (2020c). Copyright 2020, American Chemical Society.

(B) Schematic illustration of edge-attached KCl assisted growth of $MoS_2$ monolayers through a vapor–liquid–adatom–solid (VLAS) mechanism. Reprinted with permission from Huang et al. (2020). Copyright 2020, American Chemical Society.

(C) TIF-SIMS elemental mapping showing the distribution on $SiO_2$/Si substrate after CVD growth. Reprinted with permission from Li et al. (2020c). Copyright 2020, American Chemical Society.

(D) XPS core-level spectra of Na 1s in as-grown $MoS_2$ on sapphire (top) and transferred $MoS_2$ on $SiO_2$/Si substrates (bottom) through NaCl-assisted MOCVD. Reprinted with permission from Kim et al. (2017). Copyright 2017, American Chemical Society.

(E) Schematic illustration and image of 6-inch monolayer $MoS_2$ film grown on glass substrate.

(F and G) DFT-calculated energy diagrams for $MoS_2$ growth along the S-terminated edges: (F) without and (G) with Na adsorption; the blue, yellow, and purple spheres represent Mo, S, and Na atoms, respectively. Reprinted with permission from Yang et al. (2018). Copyright 2018, The Authors.

2017a). Meanwhile, atomic resolution STEM has confirmed that alkali metals are not substitutionally doped into the lattice of 2D TMDCs. Instead, they primarily adsorb on the surface of the 2D TMDCs in forms of halide salts or alkali metal-containing byproducts (Lin et al., 2021). Therefore, any residual alkali metal-containing compounds on the 2D TMDCs can be effectively removed during the wet transfer process in DI $H_2O$ or IPA/$H_2O$ solution (Figure 5D).

It is worth noting that the excessive use of salts in SA-CVD can cause contamination and lead to inferior growth of 2D TMDCs at worst. In such cases, the as-grown films have thick byproducts, weak PL, and poor electrical performance compared to those grown under optimized conditions (Kang et al., 2015; Kim et al., 2017). The negative effects of the excessive use of alkali metals were also observed in the recent study on the CVD growth of $MoSe_2$ monolayers using mixed molten salts, $Na_2MoO_4$–$Na_2SeO_3$. The introduction of $Na_2SeO_3$ initially led to the enhanced growth of continuous $MoSe_2$ films. However, as the concentration of $Na^+$ (from $Na_2SeO_3$) increased, only isolated large $MoSe_2$ flakes were grown (Li et al., 2021b). Hence, using the optimal amount of alkali-metal content is vital to grow large-area, high-quality 2D TMDCs.

Apart from the addition of alkali metal halides or molten salts, substrates containing alkali metals, such as soda-lime glass, which are primarily composed of $SiO_2$, $Na_2O$, and CaO, can also result in such enhanced growth of 2D TMDCs. For example, Chen et al. achieved rapid growth of a large $MoSe_2$ film with a domain size of up to ~2.5 mm in 5 min on a molten glass substrate (Chen et al., 2017a). The as-grown $MoSe_2$ monolayers had a high carrier mobility of up to ~95 $cm^2$/Vs. However, as the glass substrate was in a "liquid state" at the high growth temperature of 1050°C—which is above the melting point of glass (~1000°C)—droplet-like curved surfaces and cracks were formed when the glass substrates cooled down to room temperature. Subsequently, Yang et al. reported on the low-pressure CVD growth of 6-inch monolayer $MoS_2$ films on soda-lime glass at 720°C, which is slightly below the glass transition temperature of ~730°C (Figure 5E) (Yang et al., 2018). Partially oxidized Mo foil was loaded above the glass substrates to guarantee a uniform

supply of Mo precursor. This gave rise to a 6-inch monolayer $MoS_2$ film with a large domain size of ~400 μm in 8 min. The high growth rate of $MoS_2$ on glass substrates can be understood through DFT calculations. As shown in Figures 5F and 5G, incorporating Na at the edge of the growing $MoS_2$ reduces the energy barrier for converting $Mo_2S_2$ to $Mo_2S_4$ from 0.53 eV to 0.29 eV. This lower energy barrier in the Na-assisted growth of $MoS_2$ monolayers increases the growth rate by a factor of ~17 at 1000 K. Furthermore, the low-cost $MoS_2$ films grown on glass substrates can be subjected to PMMA-mediated etching-free transfer onto rigid substrates or roll-to-roll transfer onto flexible substates. Later, the authors further demonstrated the thickness tunable growth of wedding-cake-like $MoS_2$ flakes on soda-lime glass via NaCl-coated Mo foil (Yang et al., 2019b). With the aid of NaCl, the vapor pressure of Mo precursor—$MoOCl_4$ increases significantly (Table 1j). Combined with the catalytic effect of Na from soda-lime glass, $MoS_2$ tiers can be generated layer-by-layer.

To avoid the high-cost low pressure CVD and the excess supply of TM precursors in atmospheric pressure CVD, Cai et al. developed a "dissolution–precipitation" 2D TMDC growth process by sandwiching molten salts between two glass substrates (Cai et al., 2021). First, $Na_2MoO_4$, $Na_2WO_4$, and $NaVO_3$ aqueous solutions were spin-coated on a thick bottom glass substrate, and then covered with a thin glass substrate. This combination of glass substrates and the Salt 2.0 technique provides a new approach to ensure the uniform growth of 2D TMDCs and their alloys. Notably, choosing glass substrates with proper glass transition temperatures (without deformation and maintain surface flatness) and thermal expansion coefficients (to reduce strain and eliminate cracks) are critical to ensure the successful growth of high-quality 2D TMDCs. In that sense, exploring novel growth substrates could be an important direction to achieve controllable synthesis of 2D materials that deserves more research efforts (Qin et al., 2020).

## PERSPECTIVE

2D materials, especially semiconducting 2D TMDCs, have received significant attention from academics and semiconductor industry owing to their extraordinary electrical properties at monolayer (sub-nanometer) thickness. Intensive research on SA-CVD has demonstrated that it has significant potential for application in future electronics (Li et al., 2020a; Sebastian et al., 2021; Shen et al., 2021; Wang et al., 2019b). Depending on the growth modes, the SA-CVD has been generally categorized into the Salt 1.0 and Salt 2.0 techniques. Because each has its pros and cons as discussed here and other review articles (Han et al., 2019; Jiang et al., 2019; Kim et al., 2019; Xie et al., 2020), more efforts should be attributed for understanding the kinetic processes and exact roles of halogens and alkali metals in the SA-CVD growth of 2D TMDCs. Only with a more comprehensive knowledge obtained on the growth mechanisms of SA-CVD and the exact requirements for target application, proper growth techniques can be designed. The following are some promising aspects that deserve more research efforts in future.

1) Alkali-metal free growth of 2D TMDCs. To meet the critical requirements in electronics, it is of utmost importance to achieve high purity growth with extreme crystallinity. Therefore, the TM precursors have to be carefully chosen. For instance, metal organic precursors in the commonly used MOCVD system often cause carbon contamination in the as-grown 2D TMDCs (Cohen et al., 2020). On the other hand, the SA-CVD, which uses alkali-metal-free metal halides/oxyhalides (e.g., $MoCl_5$, $CrCl_3$, $FeCl_2$, $MoOCl_4$, $WO_2Cl_2$, etc.), has proven promising to eliminate the detrimental effects of alkali metals (Chu et al., 2019; Hu et al., 2021; Meng et al., 2021; Okada et al., 2014; Wang et al., 2021; Zhang et al., 2019). Replacing the metal organic precursors with the TM halides/oxyhalides in the MOCVD system could be a good alternative to realize high quality growth of 2D TMDC monolayers.

2) Low-temperature growth of 2D TMDCs. The low melting point and high vapor pressure of TM halides/oxyhalides is advantageous for low-temperature growth. This enables possible direct integration of 2D TMDCs on device wafers and even flexible substrates without transfer. In addition, it may also allow the sequential growth of TMDC-based heterojunctions without causing thermal degradation or etching of the existing TMDCs grown. With that, high-quality TMDC-based van der Waals and in-plane heterojunctions having ideal optical and electrical properties can be synthesized, and hence extending their application in related fields.

3) Layer-controlled growth of 2D TMDCs. Few-layer 2D TMDCs are more robust channel materials of FETs compared to their monolayer counterparts. This is due to their high mechanical and chemical stability that are insensitive to the intense device fabrication process. Besides, the greater number of layers also means they have more transport channels, granting them superior electrical performance

with high on-state current and carrier mobility. Because the epitaxial growth of a second TMDC layer on preexisting one has been demonstrated using molten salts (e.g., $Na_2Mo_2O_7$) (Chang et al., 2020; Li et al., 2018), there is a great potential to achieve wafer-scale layer-controlled 2D TMDCs by depositing these molten salts onto the TMDC monolayers as nucleation seeds and using TM halides/oxyhalides as main growth precursors.

4) Patterned growth and controllable doping of 2D TMDCs. Molten salts (e.g., $Na_2MoO_4$, $Na_2MoO_4$) and mixed molten salts ($Na_2WO_4$–$NaVO_3$) have been employed to grow intrinsic semiconducting 2D TMDCs and metallic V-doped/alloyed 2D TMDCs, respectively. They are ideal channel and contact/interconnecting materials for FETs and integrated circuits (ICs). Therefore, sophisticated 2D TMDC-based ICs can be fabricated using prepatterned molten salts. Meanwhile, additional research is required to explore the feasibility of using n-type dopants for growing metallic 2D TMDC alloys. This would enable the fabrication of 2D TMDC-based CMOS with p-type and n-type van der Waals contact or in-plane heterojunction, and further enrich the functionality of 2D TMDC-based ICs.

5) Wafer-scale growth of 2D TMDC single crystals. The synthesis of large-area TMDC single crystals with unprecedented crystallinity, electrical quality, and wafer-scale uniformity is the ultimate target that will eventually pave the way for 2D TMDC-based electronics (Li et al., 2021; Xu et al., 2021). Molten salts such as $Na_2Mo_2O_7$ had been used to achieve ledge-induced epitaxial growth of 1D $MoS_2$ nanoribbons along with the surface steps of NaCl crystals. Therefore, there is a great potential to synthesize wafer-scale 2D TMDC single crystals via the stitching of parallel 1D TMDC nanoribbons, which grow on engineered substrates with parallel surface steps using molten salts (Zhang et al., 2021b).

## CONCLUSIONS

Owing to the rapid development in SA-CVD, a great variety of 2D materials have been synthesized in recent years. The roles of halogen and alkali metal in promoting the growth of 2D TMDCs are elaborated herein. In general, halogens increase the volatility of the metal precursors, which have high melting points, to initiate rapid VSS growth. In contrast, alkali metals liquefy and stabilize metal precursors to achieve VLS growth. Based on the Salt 1.0 and Salt 2.0 techniques, new advanced synthetic methods could be anticipated to realize the fabrication of perfect 2D TMDCs in future for a diverse application in electronics and optoelectronics.

## ACKNOWLEDGMENTS

S. Li acknowledges the support from JSPS-KAKENHI (21K04839) and ICYS. S. Li thanks H.E. Lim (Tokyo Metropolitan University, Japan) and S. Liu (Hunan University, China) for the helpful discussion; and X. Wang (National University of Singapore, Singapore) for preparing the illustration of Figure 1I.

## REFERENCES

Arreola, V.M.A., Salazar, M.F., Zhang, T., Wang, K., Aguilar, A.H.B., Reddy, K.C.S., Strupiechonski, E., Terrones, M., and Bugallo, A.D.L. (2021). Direct growth of monolayer 1T–2H $MoS_2$ heterostructures using KCl-assisted CVD process. 2D Mater. *8*, 025033.

Bai, X., Li, S., Das, S., Du, L., Dai, Y., Yao, L., Raju, R., Du, M., Lipsanen, H., and Sun, Z. (2021). Single-step chemical vapour deposition of anti-pyramid $MoS_2$/$WS_2$ vertical heterostructures. Nanoscale *13*, 4537–4542.

Cai, Z., Lai, Y., Zhao, S., Zhang, R., Tan, J., Feng, S., Zou, J., Tang, L., Lin, J., and Liu, B. (2021). Dissolution-precipitation growth of uniform and clean two dimensional transition metal dichalcogenides. Natl. Sci. Rev. *8*, nwaa115.

Cai, Z., Shen, T., Zhu, Q., Feng, S., Yu, Q., Liu, J., Tang, L., Zhao, Y., Wang, J., and Liu, B. (2020). Dual-additive assisted chemical vapor deposition for the growth of Mn-doped 2D $MoS_2$ with tunable electronic properties. Small *16*, 1903181.

Chang, M.-C., Ho, P.-H., Tseng, M.-F., Lin, F.-Y., Hou, C.-H., Lin, I.-K., Wang, H., Huang, P.-P., Chiang, C.-H., and Yang, Y.-C. (2020). Fast growth of large-grain and continuous $MoS_2$ films through a self-capping vapor–liquid–solid method. Nat. Commun. *11*, 3682.

Chen, J., Zhao, X., Tan, S.J., Xu, H., Wu, B., Liu, B., Fu, D., Fu, W., Geng, D., and Liu, Y. (2017a). Chemical vapor deposition of large-size monolayer $MoSe_2$ crystals on molten glass. J. Am. Chem. Soc. *139*, 1073–1076.

Chen, K., Chen, Z., Wan, X., Zheng, Z., Xie, F., Chen, W., Gui, X., Chen, H., Xie, W., and Xu, J. (2017b). A simple method for synthesis of high-quality millimeter-scale 1T′ transition-metal telluride and near-field nanooptical properties. Adv. Mater. *29*, 1700704.

Chu, J., Zhang, Y., Wen, Y., Qiao, R., Wu, C., He, P., Yin, L., Cheng, R., Wang, F., and Wang, Z. (2019). Sub-millimeter-scale growth of one-unit-cell-thick ferrimagnetic $Cr_2S_3$ nanosheets. Nano Lett. *19*, 2154–2161.

Cohen, A., Patsha, A., Mohapatra, P.K., Kazes, M., Ranganathan, K., Houben, L., Oron, D., and Ismach, A. (2020). Growth-etch metal–organic chemical vapor deposition approach of $WS_2$ atomic layers. ACS Nano *15*, 526–538.

Cun, H., Macha, M., Kim, H., Liu, K., Zhao, Y., LaGrange, T., Kis, A., and Radenovic, A. (2019). Wafer-scale MOCVD growth of monolayer $MoS_2$ on sapphire and $SiO_2$. Nano Res. *12*, 2646–2652.

Fan, S., Yun, S.J., Yu, W.J., and Lee, Y.H. (2020). Tailoring quantum tunneling in a vanadium-doped $WSe_2$/$SnSe_2$ heterostructure. Adv. Sci. *7*, 1902751.

Fu, L., Hu, D., Mendes, R.G., Rümmeli, M.H., Dai, Q., Wu, B., Fu, L., and Liu, Y. (2018a). Highly organized epitaxy of Dirac semimetallic $PtTe_2$ crystals with extrahigh conductivity and visible surface plasmons at edges. ACS Nano *12*, 9405–9411.

Fu, Q., Wang, X., Zhou, J., Xia, J., Zeng, Q., Lv, D., Zhu, C., Wang, X., Shen, Y., and Li, X. (2018b).

One-step synthesis of metal/semiconductor heterostructure $NbS_2/MoS_2$. Chem. Mater. *30*, 4001–4007.

Furchi, M.M., Pospischil, A., Libisch, F., Burgdörfer, J., and Mueller, T. (2014). Photovoltaic effect in an electrically tunable van der Waals heterojunction. Nano Lett. *14*, 4785–4791.

Gao, Z., Ji, Q., Shen, P.-C., Han, Y., Leong, W.S., Mao, N., Zhou, L., Su, C., Niu, J., and Ji, X. (2018). In situ-generated volatile precursor for CVD growth of a semimetallic 2D dichalcogenide. ACS Appl. Mater. Inter. *10*, 34401–34408.

Han, S.W., Yun, W.S., Woo, W.J., Kim, H., Park, J., Hwang, Y.H., Nguyen, T.K., Le, C.T., Kim, Y.S., and Kang, M. (2021). Interface defect engineering of a large-scale CVD-grown $MoS_2$ monolayer via residual sodium at the $SiO_2$/Si substrate. Adv. Mater. Inter. *8*, 2100428.

Han, G.H., Kybert, N.J., Naylor, C.H., Lee, B.S., Ping, J., Park, J.H., Kang, J., Lee, S.Y., Lee, Y.H., and Agarwal, R. (2015). Seeded growth of highly crystalline molybdenum disulphide monolayers at controlled locations. Nat. Commun. *6*, 6128.

Han, W., Liu, K., Yang, S., Wang, F., Su, J., Jin, B., Li, H., and Zhai, T. (2019). Salt-assisted chemical vapor deposition of two-dimensional materials. Sci. China Chem. *62*, 1300–1311.

Hoang, A.T., Shinde, S.M., Katiyar, A.K., Dhakal, K.P., Chen, X., Kim, H., Lee, S.W., Lee, Z., and Ahn, J.-H. (2018). Orientation-dependent optical characterization of atomically thin transition metal ditellurides. Nanoscale *10*, 21978–21984.

Hu, D., Ye, C., Wang, X., Zhao, X., Kang, L., Liu, J., Duan, R., Cao, X., He, Y., and Hu, J. (2021). Chemical vapor deposition of superconducting $FeTe_{1-x}$ $Se_x$ nanosheets. Nano Lett. *21*, 5338–5344.

Hu, X., Huang, P., Jin, B., Zhang, X., Li, H., Zhou, X., and Zhai, T. (2018). Halide-induced self-limited growth of ultrathin nonlayered Ge flakes for high-performance phototransistors. J. Am. Chem. Soc. *140*, 12909–12914.

Huang, J.-K., Pu, J., Hsu, C.-L., Chiu, M.-H., Juang, Z.-Y., Chang, Y.-H., Chang, W.-H., Iwasa, Y., Takenobu, T., and Li, L.-J. (2014). Large-area synthesis of highly crystalline $WSe_2$ monolayers and device applications. ACS Nano *8*, 923–930.

Huang, L., Thi, Q.H., Zheng, F., Chen, X., Chu, Y.W., Lee, C.-S., Zhao, J., and Ly, T.H. (2020). Catalyzed kinetic growth in two-dimensional $MoS_2$. J. Am. Chem. Soc. *142*, 13130–13135.

Ji, Q., Zhang, Y., Gao, T., Zhang, Y., Ma, D., Liu, M., Chen, Y., Qiao, X., Tan, P.-H., and Kan, M. (2013). Epitaxial monolayer $MoS_2$ on mica with novel photoluminescence. Nano Lett. *13*, 3870–3877.

Jiang, J., Li, N., Zou, J., Zhou, X., Eda, G., Zhang, Q., Zhang, H., Li, L.-J., Zhai, T., and Wee, A.T. (2019). Synergistic additive-mediated CVD growth and chemical modification of 2D materials. Chem. Soc. Rev. *48*, 4639–4654.

Jin, Y., Zeng, Z., Xu, Z., Lin, Y.-C., Bi, K., Shao, G., Hu, T.S., Wang, S., Li, S., and Suenaga, K. (2019). Synthesis and transport properties of degenerate p-type Nb-doped $WS_2$ monolayers. Chem. Mater. *31*, 3534–3541.

Kang, K., Xie, S., Huang, L., Han, Y., Huang, P.Y., Mak, K.F., Kim, C.-J., Muller, D., and Park, J. (2015). High-mobility three-atom-thick semiconducting films with wafer-scale homogeneity. Nature *520*, 656–660.

Kappera, R., Voiry, D., Yalcin, S.E., Branch, B., Gupta, G., Mohite, A.D., and Chhowalla, M. (2014). Phase-engineered low-resistance contacts for ultrathin $MoS_2$ transistors. Nat. Mater. *13*, 1128–1134.

Kazenas, E., Tsvetkov, Y.V., Astakhova, G., Volchenkova, V., and Ovchinnikova, O. (2010). Thermodynamics of sodium molybdate evaporation. Russian Metall. (Metally) *2010*, 389–392.

Kim, H., Ovchinnikov, D., Deiana, D., Unuchek, D., and Kis, A. (2017). Suppressing nucleation in metal–organic chemical vapor deposition of $MoS_2$ monolayers by alkali metal halides. Nano Lett. *17*, 5056–5063.

Kim, M., Seo, J., Kim, J., Moon, J.S., Lee, J., Kim, J.-H., Kang, J., and Park, H. (2021). High-crystalline monolayer transition metal dichalcogenides films for wafer-scale electronics. ACS Nano *15*, 3038–3046.

Kim, S.Y., Kwak, J., Ciobanu, C.V., and Kwon, S.Y. (2019). Recent developments in controlled vapor-phase growth of 2D group 6 transition metal dichalcogenides. Adv. Mater. *31*, 1804939.

Kojima, K., Lim, H.E., Liu, Z., Zhang, W., Saito, T., Nakanishi, Y., Endo, T., Kobayashi, Y., Watanabe, K., and Taniguchi, T. (2019). Restoring the intrinsic optical properties of CVD-grown $MoS_2$ monolayers and their heterostructures. Nanoscale *11*, 12798–12803.

Lai, Z., He, Q., Tran, T.H., Repaka, D.M., Zhou, D.-D., Sun, Y., Xi, S., Li, Y., Chaturvedi, A., and Tan, C. (2021). Metastable 1T′-phase group VIB transition metal dichalcogenide crystals. Nat. Mater. *20*, 1113–1120.

Lee, C.-H., Lee, G.-H., Van Der Zande, A.M., Chen, W., Li, Y., Han, M., Cui, X., Arefe, G., Nuckolls, C., and Heinz, T.F. (2014). Atomically thin p–n junctions with van der Waals heterointerfaces. Nat. Nanotechnol. *9*, 676–681.

Lee, Y.H., Zhang, X.Q., Zhang, W., Chang, M.T., Lin, C.T., Chang, K.D., Yu, Y.C., Wang, J.T.W., Chang, C.S., and Li, L.J. (2012). Synthesis of large-area $MoS_2$ atomic layers with chemical vapor deposition. Adv. Mater. *24*, 2320–2325.

Li, J., Yang, X., Liu, Y., Huang, B., Wu, R., Zhang, Z., Zhao, B., Ma, H., Dang, W., and Wei, Z. (2020a). General synthesis of two-dimensional van der Waals heterostructure arrays. Nature *579*, 368–374.

Li, M.-Y., Shi, Y., Cheng, C.-C., Lu, L.-S., Lin, Y.-C., Tang, H.-L., Tsai, M.-L., Chu, C.-W., Wei, K.-H., and He, J.-H. (2015a). Epitaxial growth of a monolayer $WSe_2$–$MoS_2$ lateral p-n junction with an atomically sharp interface. Science *349*, 524–528.

Li, S., Wang, S., Tang, D.-M., Zhao, W., Xu, H., Chu, L., Bando, Y., Golberg, D., and Eda, G. (2015b). Halide-assisted atmospheric pressure growth of large $WSe_2$ and $WS_2$ monolayer crystals. Appl. Mater. Today *1*, 60–66.

Li, T., Guo, W., Ma, L., Li, W., Yu, Z., Han, Z., Gao, S., Liu, L., Fan, D., and Wang, Z. (2021). Epitaxial growth of wafer-scale molybdenum disulfide semiconductor single crystals on sapphire. Nat. Nanotechnol. *16*. https://doi.org/10.1038/s41565-021-00963-8.

Li, S., Hong, J., Gao, B., Lin, Y.C., Lim, H.E., Lu, X., Wu, J., Liu, S., Tateyama, Y., and Sakuma, Y. (2021a). Tunable doping of rhenium and vanadium into transition metal dichalcogenides for two-dimensional electronics. Adv. Sci. *8*, 2004438.

Li, S., Lin, Y.-C., Hong, J., Gao, B., Lim, H.E., Yang, X., Liu, S., Tateyama, Y., Tsukagoshi, K., and Sakuma, Y. (2021b). Mixed-salt enhanced chemical vapor deposition of two-dimensional transition metal dichalcogenides. Chem. Mater. *33*, 7301–7308.

Li, S., Lin, Y.-C., Liu, X.-Y., Hu, Z., Wu, J., Nakajima, H., Liu, S., Okazaki, T., Chen, W., and Minari, T. (2019). Wafer-scale and deterministic patterned growth of monolayer $MoS_2$ via vapor–liquid–solid method. Nanoscale *11*, 16122–16129.

Li, S., Lin, Y.-C., Zhao, W., Wu, J., Wang, Z., Hu, Z., Shen, Y., Tang, D.-M., Wang, J., and Zhang, Q. (2018). Vapour–liquid–solid growth of monolayer $MoS_2$ nanoribbons. Nat. Mater. *17*, 535–542.

Li, W., Huang, J., Han, B., Xie, C., Huang, X., Tian, K., Zeng, Y., Zhao, Z., Gao, P., and Zhang, Y. (2020b). Molten-salt-assisted chemical vapor deposition process for substitutional doping of monolayer $MoS_2$ and effectively altering the electronic structure and phononic properties. Adv. Sci. *7*, 2001080.

Li, X., Kahn, E., Chen, G., Sang, X., Lei, J., Passarello, D., Oyedele, A.D., Zakhidov, D., Chen, K.-W., and Chen, Y.-X. (2020c). Surfactant-mediated growth and patterning of atomically thin transition metal dichalcogenides. ACS Nano *14*, 6570–6581.

Lin, Y.-C., Lee, S., Yang, Y.-C., Chiu, P.-W., Lee, G.-D., and Suenaga, K. (2021). Two-dimensional iodine-monofluoride epitaxy on $WSe_2$. NPJ 2D Mater. Appl. *5*, 18.

Ling, X., Lee, Y.-H., Lin, Y., Fang, W., Yu, L., Dresselhaus, M.S., and Kong, J. (2014). Role of the seeding promoter in $MoS_2$ growth by chemical vapor deposition. Nano Lett. *14*, 464–472.

Ling, X., Lin, Y., Ma, Q., Wang, Z., Song, Y., Yu, L., Huang, S., Fang, W., Zhang, X., and Hsu, A.L. (2016). Parallel stitching of 2D materials. Adv. Mater. *28*, 2322–2329.

Liu, C., Xu, X., Qiu, L., Wu, M., Qiao, R., Wang, L., Wang, J., Niu, J., Liang, J., and Zhou, X. (2019). Kinetic modulation of graphene growth by fluorine through spatially confined decomposition of metal fluorides. Nat. Chem. *11*, 730–736.

Liu, H., Qi, G., Tang, C., Chen, M., Chen, Y., Shu, Z., Xiang, H., Jin, Y., Wang, S., and Li, H. (2020). Growth of large-area homogeneous monolayer transition-metal disulfides via a molten liquid intermediate process. ACS Appl. Mater. Interfaces *12*, 13174–13181.

Liu, K.-K., Zhang, W., Lee, Y.-H., Lin, Y.-C., Chang, M.-T., Su, C.-Y., Chang, C.-S., Li, H., Shi, Y., and Zhang, H. (2012). Growth of large-area and highly crystalline $MoS_2$ thin layers on insulating substrates. Nano Lett. *12*, 1538–1544.

Liu, L., Wu, J., Wu, L., Ye, M., Liu, X., Wang, Q., Hou, S., Lu, P., Sun, L., and Zheng, J. (2018). Phase-selective synthesis of 1T′-$MoS_2$ monolayers and heterophase bilayers. Nat. Mater. *17*, 1108–1114.

Liu, Y., Duan, X., Shin, H.-J., Park, S., Huang, Y., and Duan, X. (2021). Promises and prospects of two-dimensional transistors. Nature *591*, 43–53.

Ma, L., Zhu, J., Li, W., Huang, R., Wang, X., Guo, J., Choi, J.-H., Lou, Y., Wang, D., and Zou, G. (2021). Immobilized precursor particle driven growth of centimeter-sized $MoTe_2$ monolayer. J. Am. Chem. Soc. *143*, 13314–13324.

Meng, L., Zhou, Z., Xu, M., Yang, S., Si, K., Liu, L., Wang, X., Jiang, H., Li, B., and Qin, P. (2021). Anomalous thickness dependence of Curie temperature in air-stable two-dimensional ferromagnetic 1T-$CrTe_2$ grown by chemical vapor deposition. Nat. Commun. *12*, 809.

Mo, H., Zhang, X., Liu, Y., Kang, P., Nan, H., Gu, X., Ostrikov, K.K., and Xiao, S. (2019). Two-dimensional alloying molybdenum tin disulfide monolayers with fast photoresponse. ACS Appl. Mater. Inter. *11*, 39077–39087.

Najmaei, S., Liu, Z., Zhou, W., Zou, X., Shi, G., Lei, S., Yakobson, B.I., Idrobo, J.-C., Ajayan, P.M., and Lou, J. (2013). Vapour phase growth and grain boundary structure of molybdenum disulphide atomic layers. Nat. Mater. *12*, 754–759.

Naylor, C.H., Parkin, W.M., Gao, Z., Kang, H., Noyan, M., Wexler, R.B., Tan, L.Z., Kim, Y., Kehayias, C.E., and Streller, F. (2017). Large-area synthesis of high-quality monolayer 1T′-$WTe_2$ flakes. 2D Mater. *4*, 021008.

Naylor, C.H., Parkin, W.M., Ping, J., Gao, Z., Zhou, Y.R., Kim, Y., Streller, F., Carpick, R.W., Rappe, A.M., and Drndic, M. (2016). Monolayer single-crystal 1T′-$MoTe_2$ grown by chemical vapor deposition exhibits weak antilocalization effect. Nano Lett. *16*, 4297–4304.

Novoselov, K.S., Geim, A.K., Morozov, S.V., Jiang, D., Zhang, Y., Dubonos, S.V., Grigorieva, I.V., and Firsov, A.A. (2004). Electric field effect in atomically thin carbon films. Science *306*, 666–669.

Novoselov, K.S., Jiang, D., Schedin, F., Booth, T., Khotkevich, V., Morozov, S., and Geim, A.K. (2005). Two-dimensional atomic crystals. Proc. Natl. Acad. Sci. *102*, 10451–10453.

Okada, M., Sawazaki, T., Watanabe, K., Taniguch, T., Hibino, H., Shinohara, H., and Kitaura, R. (2014). Direct chemical vapor deposition growth of $WS_2$ atomic layers on hexagonal boron nitride. ACS Nano *8*, 8273–8277.

Qin, B., Ma, H., Hossain, M., Zhong, M., Xia, Q., Li, B., and Duan, X. (2020). Substrates in the synthesis of two-dimensional materials via chemical vapor deposition. Chem. Mater. *32*, 10321–10347.

Qin, Z., Loh, L., Wang, J., Xu, X., Zhang, Q., Haas, B., Alvarez, C., Okuno, H., Yong, J.Z., and Schultz, T. (2019). Growth of Nb-doped monolayer $WS_2$ by liquid-phase precursor mixing. ACS Nano *13*, 10768–10775.

Radisavljevic, B., Radenovic, A., Brivio, J., Giacometti, V., and Kis, A. (2011). Single-layer $MoS_2$ transistors. Nat. Nanotechnol. *6*, 147–150.

Rasouli, H.R., Mehmood, N., Çakıroğlu, O., and Kasırga, T.S. (2019). Real time optical observation and control of atomically thin transition metal dichalcogenide synthesis. Nanoscale *11*, 7317–7323.

Sasaki, S., Kobayashi, Y., Liu, Z., Suenaga, K., Maniwa, Y., Miyauchi, Y., and Miyata, Y. (2016). Growth and optical properties of Nb-doped $WS_2$ monolayers. Appl. Phys. Express *9*, 071201.

Schmidt, P., Binnewies, M., Glaum, R., and Schmidt, M. (2013). Chemical vapor transport reactions–methods, materials, modeling. Adv. Top. Cryst. Growth, 227–305.

Sebastian, A., Pendurthi, R., Choudhury, T.H., Redwing, J.M., and Das, S. (2021). Benchmarking monolayer $MoS_2$ and $WS_2$ field-effect transistors. Nat. Commun. *12*, 693.

Shao, G., Lu, Y., Hong, J., Xue, X.X., Huang, J., Xu, Z., Lu, X., Jin, Y., Liu, X., and Li, H. (2020). Seamlessly splicing metallic $Sn_xMo_{1-x}S_2$ at $MoS_2$ edge for enhanced photoelectrocatalytic performance in microreactor. Adv. Sci. *7*, 2002172.

Shao, G., Xue, X.-X., Zhou, X., Xu, J., Jin, Y., Qi, S., Liu, N., Duan, H., Wang, S., and Li, S. (2019). Shape-engineered synthesis of atomically thin 1T-$SnS_2$ catalyzed by potassium halides. ACS Nano *13*, 8265–8274.

Shen, P.-C., Su, C., Lin, Y., Chou, A.-S., Cheng, C.-C., Park, J.-H., Chiu, M.-H., Lu, A.-Y., Tang, H.-L., and Tavakoli, M.M. (2021). Ultralow contact resistance between semimetal and monolayer semiconductors. Nature *593*, 211–217.

Song, J.-G., Ryu, G.H., Kim, Y., Woo, W.J., Ko, K.Y., Kim, Y., Lee, C., Oh, I.-K., Park, J., and Lee, Z. (2017). Catalytic chemical vapor deposition of large-area uniform two-dimensional molybdenum disulfide using sodium chloride. Nanotechnology *28*, 465103.

Su, S.-K., Chuu, C.-P., Li, M.-Y., Cheng, C.-C., Wong, H.-S.P., and Li, L.-J. (2021). Layered semiconducting 2D materials for future transistor applications. Small Struct. *2*, 2000103.

Sung, J.H., Heo, H., Si, S., Kim, Y.H., Noh, H.R., Song, K., Kim, J., Lee, C.-S., Seo, S.-Y., and Kim, D.-H. (2017). Coplanar semiconductor–metal circuitry defined on few-layer $MoTe_2$ via polymorphic heteroepitaxy. Nat. Nanotechnol. *12*, 1064–1070.

Tan, J., Li, S., Liu, B., and Cheng, H.-M. (2021). Structure, preparation, and applications of 2D material-based metal–semiconductor heterostructures. Small Struct. *2*, 2000093.

Tang, L., Xu, R., Tan, J., Luo, Y., Zou, J., Zhang, Z., Zhang, R., Zhao, Y., Lin, J., and Zou, X. (2021). Modulating electronic structure of monolayer transition metal dichalcogenides by substitutional Nb-doping. Adv. Funct. Mater. *31*, 2006941.

Voiry, D., Mohite, A., and Chhowalla, M. (2015). Phase engineering of transition metal dichalcogenides. Chem. Soc. Rev. *44*, 2702–2712.

Voiry, D., Yamaguchi, H., Li, J., Silva, R., Alves, D.C., Fujita, T., Chen, M., Asefa, T., Shenoy, V.B., and Eda, G. (2013). Enhanced catalytic activity in strained chemically exfoliated $WS_2$ nanosheets for hydrogen evolution. Nat. Mater. *12*, 850–855.

Vu, V.T., Vu, T.T.H., Phan, T.L., Kang, W.T., Kim, Y.R., Tran, M.D., Nguyen, H.T.T., Lee, Y.H., and Yu, W.J. (2021). One-step synthesis of $NbSe_2$/Nb-doped $WSe_2$ metal/doped-semiconductor van der Waals heterostructures for doping controlled ohmic contact. ACS Nano *15*, 13031–13040.

Wang, D., Zhou, Y., Zhang, H., Zhang, R., Dong, H., Xu, R., Cheng, Z., He, Y., and Wang, Z. (2020). Wafer-scale growth of pristine and doped monolayer $MoS_2$ films for electronic device applications. Inorg. Chem. *59*, 17356–17363.

Wang, H., Chen, Y., Duchamp, M., Zeng, Q., Wang, X., Tsang, S.H., Li, H., Jing, L., Yu, T., and Teo, E.H.T. (2018). Large-area atomic layers of the charge-density-wave conductor $TiSe_2$. Adv. Mater. *30*, 1704382.

Wang, H., Huang, X., Lin, J., Cui, J., Chen, Y., Zhu, C., Liu, F., Zeng, Q., Zhou, J., and Yu, P. (2017a). High-quality monolayer superconductor $NbSe_2$ grown by chemical vapour deposition. Nat. Commun. *8*, 394.

Wang, P., Lei, J., Qu, J., Cao, S., Jiang, H., He, M., Shi, H., Sun, X., Gao, B., and Liu, W. (2019a). Mechanism of alkali metal compound-promoted growth of monolayer $MoS_2$: eutectic intermediates. Chem. Mater. *31*, 873–880.

Wang, Q.H., Kalantar-Zadeh, K., Kis, A., Coleman, J.N., and Strano, M.S. (2012). Electronics and optoelectronics of two-dimensional transition metal dichalcogenides. Nat. Nanotechnol. *7*, 699–712.

Wang, X., Bian, C., He, Y., Guo, J., Zhang, P., Liu, L., Wei, Y., Meng, L., Jiang, H., and Li, B. (2021). Ultrathin FeTe nanosheets with tetragonal and hexagonal phases synthesized by chemical vapor deposition. Mater. Today *45*, 35–43.

Wang, Y., Kim, J.C., Wu, R.J., Martinez, J., Song, X., Yang, J., Zhao, F., Mkhoyan, A., Jeong, H.Y., and Chhowalla, M. (2019b). Van der Waals contacts between three-dimensional metals and two-dimensional semiconductors. Nature *568*, 70–74.

Wang, Z., Xie, Y., Wang, H., Wu, R., Nan, T., Zhan, Y., Sun, J., Jiang, T., Zhao, Y., and Lei, Y. (2017b). NaCl-assisted one-step growth of $MoS_2$–$WS_2$ in-plane heterostructures. Nanotechnology *28*, 325602.

Xie, C., Yang, P., Huan, Y., Cui, F., and Zhang, Y. (2020). Roles of salts in the chemical vapor deposition synthesis of two-dimensional transition metal chalcogenides. Dalton Trans. *49*, 10319–10327.

Xu, D., Chen, W., Zeng, M., Xue, H., Chen, Y., Sang, X., Xiao, Y., Zhang, T., Unocic, R.R., and Xiao, K. (2018). Crystal-field tuning of photoluminescence in two-dimensional materials with embedded lanthanide ions. Angew. Chem. Int. Ed. *57*, 755–759.

Xu, X., Pan, Y., Liu, S., Han, B., Gu, P., Li, S., Xu, W., Peng, Y., Han, Z., and Chen, J. (2021). Seeded 2D epitaxy of large-area single-crystal films of the van der Waals semiconductor 2H $MoTe_2$. Science *372*, 195–200.

Yang, P., Yang, A.-G., Chen, L., Chen, J., Zhang, Y., Wang, H., Hu, L., Zhang, R.-J., Liu, R., and Qu, X.-P. (2019a). Influence of seeding promoters on the properties of CVD grown monolayer molybdenum disulfide. Nano Res. *12*, 823–827.

Yang, P., Zhang, Z., Sun, M., Lin, F., Cheng, T., Shi, J., Xie, C., Shi, Y., Jiang, S., and Huan, Y. (2019b). Thickness tunable wedding-cake-like $MoS_2$ flakes for high-performance optoelectronics. ACS Nano *13*, 3649–3658.

Yang, P., Zou, X., Zhang, Z., Hong, M., Shi, J., Chen, S., Shu, J., Zhao, L., Jiang, S., and Zhou, X. (2018). Batch production of 6-inch uniform monolayer molybdenum disulfide catalyzed by sodium in glass. Nat. Commun. *9*, 979.

Yu, Y., Nam, G.-H., He, Q., Wu, X.-J., Zhang, K., Yang, Z., Chen, J., Ma, Q., Zhao, M., and Liu, Z. (2018). High phase-purity 1T′-$MoS_2$-and 1T′-$MoSe_2$ layered crystals. Nat. Chem. *10*, 638–643.

Yun, S.J., Duong, D.L., Ha, D.M., Singh, K., Phan, T.L., Choi, W., Kim, Y.M., and Lee, Y.H. (2020). Ferromagnetic order at room temperature in monolayer $WSe_2$ semiconductor via vanadium dopant. Adv. Sci. *7*, 1903076.

Zhan, Y., Liu, Z., Najmaei, S., Ajayan, P.M., and Lou, J. (2012). Large-area vapor-phase growth and characterization of $MoS_2$ atomic layers on a $SiO_2$ substrate. Small *8*, 966–971.

Zhang, D., Wen, C., Mcclimon, J.B., Masih Das, P., Zhang, Q., Leone, G.A., Mandyam, S.V., Drndić, M., Johnson, A.T.C., Jr., and Zhao, M.Q. (2021a). Rapid growth of monolayer $MoSe_2$ films for large-srea rlectronics. Adv. Electron. Mater. *7*, 2001219.

Zhang, L., Dong, J., and Ding, F. (2021b). Strategies, status, and challenges in wafer scale single crystalline two-dimensional materials synthesis. Chem. Rev. *121*, 6321–6372.

Zhang, L., Wang, C., Liu, X.-L., Xu, T., Long, M., Liu, E., Pan, C., Su, G., Zeng, J., and Fu, Y. (2017a). Damage-free and rapid transfer of CVD-grown two-dimensional transition metal dichalcogenides by dissolving sacrificial water-soluble layers. Nanoscale *9*, 19124–19130.

Zhang, L., Wang, G., Zhang, Y., Cao, Z., Wang, Y., Cao, T., Wang, C., Cheng, B., Zhang, W., and Wan, X. (2020). Tuning electrical conductance in bilayer $MoS_2$ through defect-mediated interlayer chemical bonding. ACS Nano *14*, 10265–10275.

Zhang, Q., Xiao, Y., Zhang, T., Weng, Z., Zeng, M., Yue, S., Mendes, R.G., Wang, L., Chen, S., and Rümmeli, M.H. (2017b). Iodine-mediated chemical vapor deposition growth of metastable transition metal dichalcogenides. Chem. Mater. *29*, 4641–4644.

Zhang, K., Bersch, B.M., Zhang, F., Briggs, N.C., Subramanian, S., Xu, K., Chubarov, M., Wang, K., Lerach, J.O., and Redwing, J.M. (2018). Considerations for utilizing sodium chloride in epitaxial molybdenum disulfide. ACS Appl. Mater. Interfaces *10*, 40831–40837.

Zhang, Y., Chu, J., Yin, L., Shifa, T.A., Cheng, Z., Cheng, R., Wang, F., Wen, Y., Zhan, X., and Wang, Z. (2019). Ultrathin magnetic 2D single-crystal CrSe. Adv. Mater. *31*, 1900056.

Zhang, Y., Yin, L., Chu, J., Shifa, T.A., Xia, J., Wang, F., Wen, Y., Zhan, X., Wang, Z., and He, J. (2018). Edge-epitaxial growth of 2D $NbS_2$-$WS_2$ lateral metal-semiconductor heterostructures. Adv. Mater. *30*, 1803665.

Zhou, J., Lin, J., Huang, X., Zhou, Y., Chen, Y., Xia, J., Wang, H., Xie, Y., Yu, H., and Lei, J. (2018). A library of atomically thin metal chalcogenides. Nature *556*, 355–359.

Zou, J., Cai, Z., Lai, Y., Tan, J., Zhang, R., Feng, S., Wang, G., Lin, J., Liu, B., and Cheng, H.-M. (2021). Doping concentration modulation in vanadium-doped monolayer molybdenum disulfide for synaptic transistors. ACS Nano *15*, 7340–7347.

Zuo, Y., Yu, W., Liu, C., Cheng, X., Qiao, R., Liang, J., Zhou, X., Wang, J., Wu, M., and Zhao, Y. (2020). Optical fibres with embedded two-dimensional materials for ultrahigh nonlinearity. Nat. Nanotechnol. *15*, 987–991.